MICROSTRUCTURAL ANALYSIS OF TI-6AL-4V COMPONENTS MADE BY ELECTRON BEAM ADDITIVE MANUFACTURING

by

RASHADD L. COLEMAN

VIOLA L. ACOFF, COMMITTEE CHAIR
PAUL ALLISON
J. BRIAN JORDON
CHARLES MONROE
MARK L. WEAVER

A DISSERTATION

Submitted in partial fulfillment of the requirements
for the degree of Doctor of Philosophy in the
Department of Metallurgical and Materials
Engineering in the Graduate School of
The University of Alabama

TUSCALOOSA, ALABAMA

2017

ABSTRACT

Electron Beam Additive Manufacturing (EBAM) is a relatively new additive manufacturing (AM) technology that uses a high-energy electron beam to melt and fuse powders to build full-density parts in a layer by layer fashion. EBAM can fabricate metallic components, particularly, of complex shapes, in an efficient and cost-effective manner compared to conventional manufacturing means. EBAM is an enabling technology for rapid manufacturing (RM) of metallic components, and thus, can efficiently integrate the design and manufacturing of aerospace components. However, EBAM for aerospace-related applications remain limited because the effect of the EBAM process on part characteristics is not fully understood. In this study, various techniques including microhardness, optical microscopy (OM), X-ray diffraction (XRD), Scanning Electron Microscopy (SEM), and electron backscatter diffraction (EBSD) were used to characterize Ti-6Al-4V components processed using EBAM. The results were compared to Ti-6Al-4V components processed using conventional techniques. In this study it is shown that EBAM built Ti-64 components have increased hardness, elastic modulus, and yield strength compared to wrought Ti-6Al-4V. Further, it is also shown in this study that the horizontal build EBAM Ti-6Al-4V has increased hardness, elastic modulus, and yield strength compared to vertical build EBAM due to a preferential growth of the β phase.

DEDICATION

This dissertation is first dedicated to my Lord and Savior, Jesus Christ; for without Him none of this would be possible. Secondly, this work is dedicated to my parents Rickey and Mary Coleman whose prayer, guidance, and inspiration led to the completion of this work. This work is also dedicated to my bride-to-be Ebony Griffin; her love and support through all the nights of tears and self-doubt were invaluable throughout this process and to her I say, "The best is yet to come!"

LIST OF ABBREVIATIONS AND SYMBOLS

Ti	Titanium
α	Alpha Phase, Hexagonally Closed Packed Phase of Titanium or Titanium Alloys
Ti-64	Ti-6Al-4V
HCP	Hexagonal Close-Packed
BCC	Body Centered Cubic
β	Beta Phase, Body Centered Cubic Phase of Titanium or Titanium Alloys
α´	Martensitic structure in Titanium or Titanium alloys
β-transus	β-phase transus temperature
Al	Aluminum
V	Vanadium
EBW	Electron Beam Welding
HAZ	Heat Affected Zone
EBAM	Electron Beam Additive Manufacturing
AM	Additive Manufacturing
BoB	Bead-Over-Bead
BoBoB	Bead-Over-Bead-Over-Bead
EBM	Electron Beam Melting
MSFC	Marshall Space Flight Center
HV	Vickers Microhardness
YS	Yield Strength

UTS	Ultimate Tensile Strength
OM	Optical Microscopy
SEM	Scanning Electron Microscopy
XRD	X-Ray Diffraction
HRC	Rockwell hardness C
EBSD	Electron Back Scattered Diffraction
MTEX	Matlab Texture
ND	Normal Direction
RD	Rolling Direction
TD	Transversal Direction
BD	Build Direction
SD	Scanning Direction
IPF	Inverse Pole Figure
PF	Pole Figure
GB	Grain Boundary
CSL	Coincidence Site Lattice
LAGB	Low Angle Grain Boundary

ACKNOWLEDGEMENTS

First I'm immensely grateful to my advisor, Dr. Viola L. Acoff, for her encouragement, patience, guidance, advice, and support throughout my time here at The University of Alabama. Dr. Acoff's insight and support have had a profound influence on me personally as well as professionally and without her, I would not be where I am today. I'd like to extend my deepest appreciation to my committee members, Dr. Allison, Dr. Barkey, Dr. Jordan, Dr. Monroe, and Dr. Weaver for their invaluable suggestions and comments on this work.

I want to thank some of the friends I have made here along the way that have selflessly helped me in more ways than they'll ever know: Dr. Todd Butler, Dr. Derrick Stokes, Sharniece Holland, Brett Hunter, and Katherine Vinson. To each of them I owe a debt that I can never repay for the immeasurable impact they've had on both my research and my life. I'd also like to thank Johnny Goodwin, Rich Martens, and Rob Holler of the CAF for their invaluable help with the instrumentation in this work. I'd like to thank NASA for the financial support (Grant No. NNX11AM11A).

I gratefully acknowledge the former members of Dr. Acoff's group that I have had the personal pleasure of working alongside: Dr. Peng Qu, Dr. Kai Tan, Dr. Liming Zhou, Dr. Juzi Li, and Dr. Derrick Stokes. Their discussions, inputs, and encouragements have been a blessing to me; and it is my sincerest hope that this work will measure up to the shining examples they have set for me. Most of all, I would like to thank God; through Him, all things are possible and as it turns out, that includes finishing graduate school.

"Commit to the Lord whatever you do, and all your plans will succeed." Proverbs 16:3

CONTENTS

LIST OF TABLES

LIST OF FIGURES

CHAPTER 1

INTRODUCTION

1.1 Ti-6Al-4V

Titanium (Ti) and its alloys are used in many industries, but mostly in the aerospace and automobile industries due to its favorable combination of mechanical and chemical properties [2]. These mechanical properties are directly influenced by microstructure which is in turn directly influenced by processing and thermal treatment [3]. Ti is generally stable at certain temperature ranges. The stable phase at low temperature is α, which has a hexagonal close-packed (HCP) structure. Pure Ti undergoes a phase transformation from α to a body centered cubic (BCC) phase (β) at 882 °C, and remains stable up to the melting point. Ti alloys are usually categorized into four groups that depend on the major phase or phases present in their microstructure: α, β, α+β alloys, and intermetallics [4]. The addition of alloying elements to Ti yields a wide range of chemical and mechanical properties; Al, C, N, and O are α-stabilizers, while Mo, Nb, Ta, and V are β-stabilizers. The unit cells for α and β Ti are shown in Figure 1.1 [1].

Ti-6Al-4V (Ti-64) is the most widely used titanium alloy due to its versatile combination of strength and other mechanical properties that it retains even at high temperatures. Because of this, Ti-64 is highly used in the aeronautics and aerospace industries, but due to its biological and chemical inertness it is also used extensively in both the medical and dental industries [5-7]. Because of its corrosion resistance, Ti-64 is also used in pipes and deep-sea oil wells. RecentlyTi-64 has been used in jewelry, architecture, outdoor equipment, and sporting goods Ti-

64 has two allotropic phases present; the BCC β-phase that is stabilized by the 4% vanadium and the HCP structured α-phase that is stabilized by the 6% aluminum [8]. At room temperature, the alloy is comprised mostly of α. However, at the β transus temperature, around 980-996 °C, [9] the β-phase becomes completely stable up to the melting point [10]. A rapid cooling rate, i.e. above 137 °C/s [11] from the homogeneous β produces martensitic α-phases [12]. A slower cooling rate below the β transus temperature leads to a diffusion controlled nucleation and growth process: grain boundary α-phase may grow at the β-grain boundaries or a plate-like α´ structure may form within the prior β grains at lower temperatures [13]. The plate-like α´ structure is known as Widmanstätten

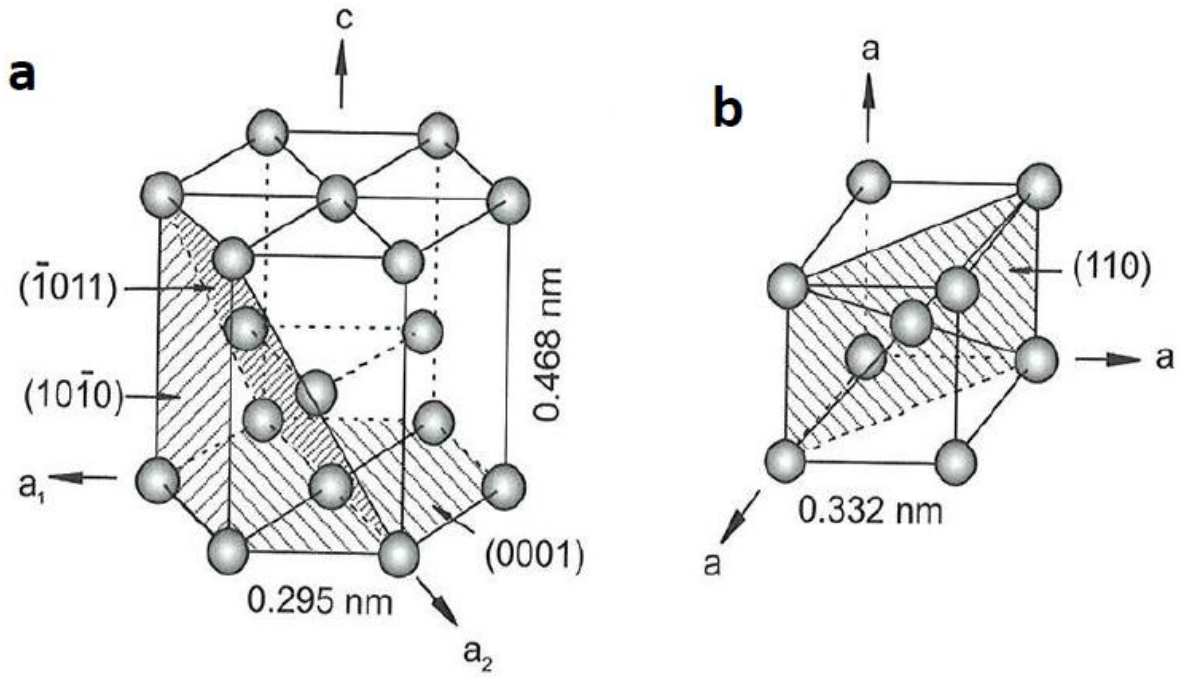

Figure 1.1 Unit cells of (a) α-phase Ti and (b) β phase Ti. *Figure adapted from [1]*.

1.2 Electron Beam Welding of Ti-64

Electron beam Welding (EBW) is a commonly used welding technique that is quite similar to the process explored in this work. For EBW, an electron beam is used to join metals. While the parent metals are largely unaffected, the weld joint and the heat affected zone (HAZ) undergo a change at the microstructural level. Because of this noteworthy similarity to electron beam additive manufacturing (EBAM), the microstructures for EBW of Ti64 found in the literature were used as a baseline for understanding the microstructures for EBAM Ti-64 in this study. In many of the EBW studies, researchers found that conventional stringer bead welding caused a reduction in Charpy impact toughness. But with more beads came an increase in many of the mechanical properties such as ultimate tensile and yield strengths as well as impact toughness and hardness at the weld and the heat affected zone (HAZ) [1,2]. The researchers believed that the multiple passes in the same weld bead caused a decrease in the overall cooling rate and thus, created more of the martensitic needle structure that is shown to be stronger than the parent material.

1.3 Additive Manufacturing

EBAM has been widely used to manufacture metals and alloys, especially titanium and its alloys. EBAM is one of the few AM (additive manufacturing) technologies capable of making full-density metallic parts in a layer-by-layer fashion and has therefore dramatically extended the applications of EBAM [3-7]. The inside of a typical EBAM machine is shown in Figure 1.2 [5]. It is important to note that the chemical composition for Ti-64 used in EBAM is different from other commercial uses, as is shown in Table 1.1 [8].

EBAM represents a promising opportunity to increase the use of titanium alloys due to its process versatility and flexibility, the non-reactive environmental requirements, and its rapid

processing and minimal waste. Furthermore, EBAM offers a more efficient and cost effective way to manufacture titanium parts. This is accomplished by a dedicated effort to improve upon the manufacturing process itself to result in a higher-quality product while simultaneously reducing processing costs once the part is completed. Therefore, the use of EBAM to process titanium alloys such as Ti-64 represents a viable means of manufacturing fully functional, net-shaped parts for aerospace and medical applications at both a cost and time efficient manner.

Since EBAM is a relatively new technology, there are still many aspects that have yet to be fully understood such as the microstructure evolution and phase transformations. The morphology of the microstructure is critical in the determination of the properties of the components and to date, it is not fully understood what effect the EBAM process has on component characteristics. The mechanical properties of titanium alloys are dependent on the microstructure, which is determined by the thermo-mechanical processing and thermal treatment.

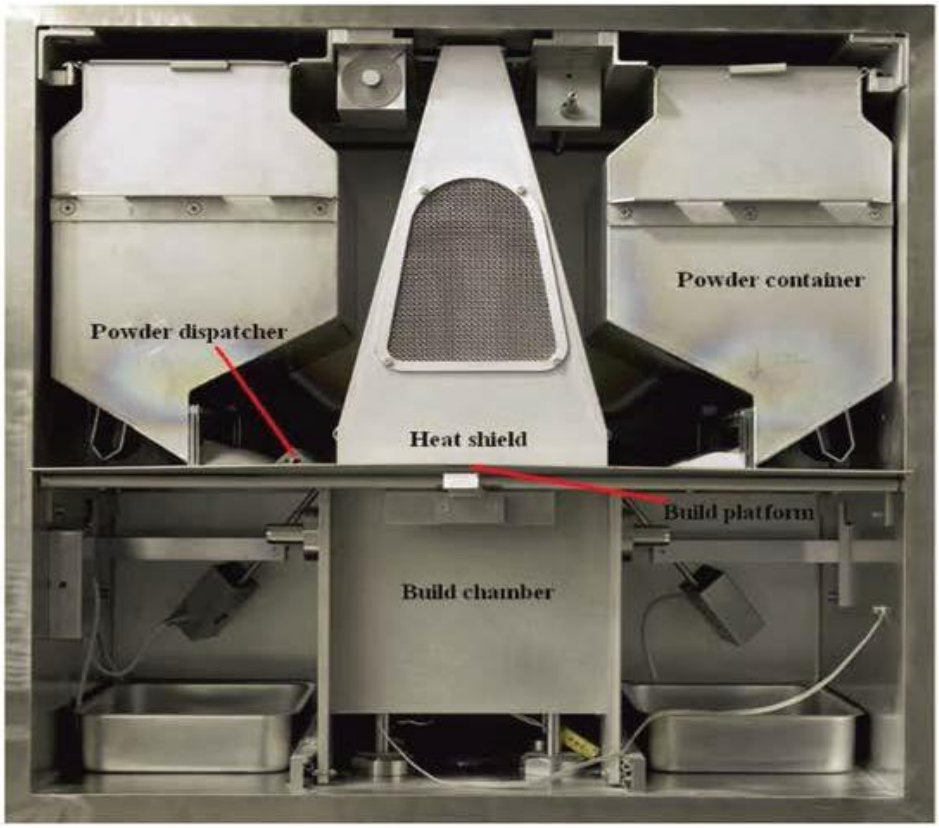

Figure 1.2 Inside of an EBAM Machine.

Table 1.1 Chemical Specification of Ti-64

	Arcam Ti6Al4V, Typical	***Ti6Al4V, (ASTM F1108; Required for Cast)***	***Ti6Al4V, (ASTM F1472; Required for Wrought)***
Aluminum, Al	**6%**	**5.5-6.75%**	**5.5-6.75%**
Vanadium, V	**4%**	**3.5-4.5%**	**3.5-4.5%**
Carbon, C	**0.03%**	**< 0.1%**	**< 0.08%**
Iron, Fe	**0.1%**	**< 0.3%**	**< 0.3%**
Oxygen, O	**0.15%**	**< 0.2%**	**< 0.2%**
Nitrogen, N	**0.01%**	**< 0.5%**	**< 0.05%**
Hydrogen, H	**0.003%**	**< 0.015%**	**< 0.015%**
Titanium, Ti	**Balance**	**Balance**	**Balance**

1.4 Background and Motivation

As previously stated, the mechanical properties of titanium alloys are dependent upon microstructure, which in turn is dependent upon thermo-mechanical processing and thermal treatments [1-4,9-18]. One aim of this research is to identify some the mechanical properties present in Ti-64 fabricated by EBAM and the resultant microstructural evolution. However the main goal of this work is to directly compare these results to those of a conventional wrought Ti-64.

Grain and colony size of α/β Ti alloys is still a hotly debated topic. There are several different standards already in use for characterizing grain and colony size based on images. However, the quantification of microstructural features in α/β Ti alloys is extremely difficult [19]. There are two main reasons to explain the difficulty. Firstly, the microstructure of Ti-64 is complex and contains features that span a wide range of size scales: from sub-micron to the order of millimeters. Secondly, the information available from a two-dimensional section of the micrograph is insufficient to understand three-dimensional aspects. Therefore without making assumptions about shape and morphology, determining size is difficult [20]. This work does not aim to settle the debate, but merely to contribute to the available data. We will also investigate if there is a preferred direction for grain growth as a function of processing parameters (i.e. build direction).

References

[1] K. P. Rao, K. Angamuthu and P. B. Srinivasan, "Fracture toughness of electron beam welded Ti6Al4V," *Journal of Materials Processing Technology* 199 (2008) 185-192.

[2] S. Wang and X. Wu, "Investigation on the microstructure and mechanical properties of Ti–6Al–4V alloy joints with electron beam welding," *Materials & Design* 36 (2012) 663-670.

[3] W. E. Frazier, "Metal Additive Manufacturing: A Review," *Journal of Materials Engineering and Performance* 23 (2014) 1917-1928.

[4] L. E. Murr, E. Martinez, K. N. Amato, S. M. Gaytan, J. Hernandez, D. A. Ramirez, P. W. Shindo, F. Medina and R. B. Wicker, "Fabrication of Metal and Alloy Components by Additive Manufacturing: Examples of 3D Materials Science," *Journal of Materials Research and Technology* 1 (2012) 42-54.

[5] V. Petrovic, J. Vicente Haro Gonzalez, O. Jordá Ferrando, J. Delgado Gordillo, J. Ramón Blasco Puchades and L. Portolés Griñan, "Additive layered manufacturing: sectors of industrial application shown through case studies," *International Journal of Production Research* 49 (2011) 1061-1079.

[6] S. Biamino, A. Penna, U. Ackelid, S. Sabbadini, O. Tassa, P. Fino, M. Pavese, P. Gennaro and C. Badini, "Electron beam melting of Ti–48Al–2Cr–2Nb alloy: Microstructure and mechanical properties investigation," *Intermetallics* 19 (2011) 776-781.

[7] L. E. Murr, S. M. Gaytan, D. A. Ramirez, E. Martinez, J. Hernandez, K. N. Amato, P. W. Shindo, F. R. Medina and R. B. Wicker, "Metal Fabrication by Additive Manufacturing Using Laser and Electron Beam Melting Technologies," *Journal of Materials Science & Technology* 28 (2012) 1-14.

[8] Arcam, "Ti6Al4V Titanium Alloy." Arcam AB. http://www.arcam.com/wp-content/uploads/Arcam-Ti6Al4V-Titanium-Alloy.pdf. Accessed May 9 2016

[9] C. Charles, "Modelling microstructure evolution of weld deposited Ti-6Al-4V," *Thesis, Luleå University of Technology* (2008).

[10] R. Ding, Z. X. Guo and A. Wilson, "Microstructural Evolution of a Ti–6Al–4V Alloy During Thermomechanical Processing," *Materials Science and Engineering: A* 327 (2002) 233-245.

[11] L. Facchini, E. Magalini, P. Robotti and A. Molinari, "Microstructure and mechanical properties of Ti-6Al-4V produced by electron beam melting of pre-alloyed powders," *Rapid Prototyping Journal* 15 (2009) 171-178.

[12] J. Karlsson, A. Snis, H. Engqvist and J. Lausmaa, "Characterization and comparison of materials produced by Electron Beam Melting (EBM) of two different Ti–6Al–4V powder fractions," *Journal of Materials Processing Technology* 213 (2013) 2109-2118.

[13] N. Hrabe and T. Quinn, "Effects of processing on microstructure and mechanical properties of a titanium alloy (Ti–6Al–4V) fabricated using electron beam melting (EBM), part 1: Distance from build plate and part size," *Materials Science and Engineering: A* 573 (2013) 264-270.

[14] A. Majorell, S. Srivatsa and R. R. Picu, "Mechanical Behavior of Ti-6Al-4V at High and Moderate Temperatures," *Materials Science and Engineering: A* 326 (2002) 297 297-305.

[15] J. Parthasarathy, B. Starly, S. Raman and A. Christensen, "Mechanical evaluation of porous titanium (Ti6Al4V) structures with electron beam melting (EBM)," *Journal of the mechanical behavior of biomedical materials* 3 (2010) 249-259.

[16] Y. Zhai, H. Galarraga and D. A. Lados, "Microstructure Evolution, Tensile Properties, and Fatigue Damage Mechanisms in Ti-6Al-4V Alloys Fabricated by Two Additive Manufacturing Techniques," *Procedia Engineering* 114 (2015) 658-666.

[17] L. E. Murr, E. V. Esquivel, S. A. Quinones, S. M. Gaytan, M. I. Lopez, E. Y. Martinez, F. Medina, D. H. Hernandez, E. Martinez, J. L. Martinez, S. W. Stafford, D. K. Brown, T. Hoppe, W. Meyers, U. Lindhe and R. B. Wicker, "Microstructures and mechanical properties of electron beam-rapid manufactured Ti–6Al–4V biomedical prototypes compared to wrought Ti–6Al–4V," *Materials Characterization* 60 (2009) 96-105.

[18] C. C. Murgau, R. Pederson and L. E. Lindgren, "A model for Ti–6Al–4V microstructure evolution for arbitrary temperature changes," *Modelling and Simulation in Materials Science and Engineering* 20 (2012) 055006.

[19] J. Tiley, T. Searles, E. Lee, S. Kar, R. Banerjee, J. C. Russ and H. L. Fraser, "Quantification of microstructural features in α/β titanium alloys," *Materials Science and Engineering: A* 372 (2004) 191-198.

[20] T. Searles, J. Tiley, A. Tanner, R. Williams, B. Rollins, E. Lee, S. Kar, R. Banerjee and H. L. Fraser, "Rapid characterization of titanium microstructural features for specific modelling of mechanical properties," *Measurement Science and Technology* 16 (2005) 60-69.

CHAPTER 2

RESEARCH OBJECTIVES AND ORGANIZATION

Ti-64 was originally designed to be a wrought alloy and casting, forging and machining are used to manufacture titanium products [1]. It is well known that processing determines microstructure and that in turn determines properties [2-8]. While the properties of wrought Ti-64 are well known, this work will further elucidate the microstructures of Ti-64 components processed by EBAM and compare the microstructures to the already understood microstructures of wrought Ti-64 and by doing so, this work also aims to show that the EBAM process produces microstructural properties in Ti-64 that are as good or better than those of wrought Ti-64. To that end, the overall the objectives of this dissertation are devoted to:

(1) The microstructural evolution due to the EBAM process and its effect on the mechanical properties of Ti-64.
(2) XRD and preferential β grain growth as a function of build direction.
(3) Texture, microstructural modeling and EBSD simulation of EBAM Ti-64.

2.1 Dissertation Organization

This is an article-based dissertation. Each chapter consists of an article that is ready for submission for publication. Chapter 3 presents the microscopy and microhardness of Ti-64 components made by EBAM and directly compares the results with those of wrought Ti-64. In Chapter 4, XRD and preferential grain growth as a function of build direction (i.e. vertical and horizontal) is investigated. The preferential growth affects mechanical properties with respect to

build direction. In addition, failure modes of Ti-64 are investigated via SEM. Chapter 5 is devoted to EBSD with an emphasis on texture modeling and analysis of the Ti-64 microstructure.

References

[1] M. Shunmugavel, A. Polishetty and G. Littlefair, "Microstructure and mechanical properties of wrought and additive manufactured Ti-6Al-4V cylindrical bars," *Procedia Technology* 20 (2015) 231-236.

[2] W. E. Frazier, "Metal Additive Manufacturing: A Review," *Journal of Materials Engineering and Performance* 23 (2014) 1917-1928.

[3] R. Ding, Z. X. Guo and A. Wilson, "Microstructural Evolution of a Ti–6Al–4V Alloy During Thermomechanical Processing," *Materials Science and Engineering: A* 327 (2002) 233-245.

[4] A. Majorell, S. Srivatsa and R. R. Picu, "Mechanical Behavior of Ti-6Al-4V at High and Moderate Temperatures," *Materials Science and Engineering: A* 326 (2002) 297 297-305.

[5] C. C. Murgau, R. Pederson and L. E. Lindgren, "A model for Ti–6Al–4V microstructure evolution for arbitrary temperature changes," *Modelling and Simulation in Materials Science and Engineering* 20 (2012) 055006.

[6] L. E. Murr, E. V. Esquivel, S. A. Quinones, S. M. Gaytan, M. I. Lopez, E. Y. Martinez, F. Medina, D. H. Hernandez, E. Martinez, J. L. Martinez, S. W. Stafford, D. K. Brown, T. Hoppe, W. Meyers, U. Lindhe and R. B. Wicker, "Microstructures and mechanical properties of electron beam-rapid manufactured Ti–6Al–4V biomedical prototypes compared to wrought Ti–6Al–4V," *Materials Characterization* 60 (2009) 96-105.

[7] L. E. Murr, S. M. Gaytan, D. A. Ramirez, E. Martinez, J. Hernandez, K. N. Amato, P. W. Shindo, F. R. Medina and R. B. Wicker, "Metal Fabrication by Additive Manufacturing Using Laser and Electron Beam Melting Technologies," *Journal of Materials Science & Technology* 28 (2012) 1-14.

[8] S. Wang and X. Wu, "Investigation on the microstructure and mechanical properties of Ti–6Al–4V alloy joints with electron beam welding," *Materials & Design* 36 (2012) 663-670.

CHAPTER 3

MICROHARDNESS AND MICROSCOPY OF TI-6AL-4V COMPONENTS MADE BY ELECTRON BEAM ADDITIVE MANUFACTURING

Abstract

Electron Beam Additive Manufacturing (EBAM) is a relatively new additive manufacturing (AM) technology that uses a high-energy electron beam to melt and fuse powders to build full-density parts in a layer by layer fashion. EBAM can fabricate metallic components, particularly, of complex shapes, in an efficient and cost-effective manner compared to conventional manufacturing means. EBAM is an enabling technology for rapid manufacturing (RM) of metallic components, and thus, can efficiently integrate the design and manufacturing of aerospace components. However, EBAM for aerospace-related applications remain limited because the effect of the EBAM process on part characteristics is not fully understood. In this study, the microscopy and hardness of Ti-6Al-4V (Ti-64) components made by EBAM were investigated and compared to those of wrought Ti-64 components.

3.1 Introduction

Electron beam additive manufacturing (EBAM) is a relatively new additive manufacturing (AM) technique that is able to build full density parts in a layer-by-layer fashion using an electron beam to melt and fuse powders. AM techniques use 3D model data to build layer upon layer and are thus different from subtractive manufacturing techniques where material is removed [1]. Electron beam melting (EBM) is one of the few AM technologies capable of making full-density metallic parts and has therefore dramatically extended its applications [1-5]. Since EBM is a relatively new technology, there are still many aspects that have yet to be fully understood such as the microstructure evolution and phase transformation. The morphology of the microstructure is critical in the determination of the properties of the components and to date, it is not fully understood what effect the EBAM process has on component characteristics. The mechanical properties of titanium alloys are dependent on the microstructure, which is determined by the thermo-mechanical processing and thermal treatment. The main focus of this study is to investigate the microstructure of Ti-64 components made by EBAM and directly compare the observed microstructure to Ti-64 components made by conventional means.

The Ti-6Al-4V (Ti-64) alloy has an excellent combination of properties such as corrosion resistance, a high strength-to-weight ratio and low density that have made it the material of choice in many industrial applications including aerospace [6]. Ti-64 has two allotropic phases present: the body centered cubic (BCC) β-phase that is stabilized by the 4% vanadium and the hexagonal close-packed (HCP) structured α-phase that is stabilized by the 6% aluminum [7,8]. The mechanical properties of titanium alloys are dependent upon microstructure, which in turn is dependent upon thermo-mechanical processing and thermal treatments [1,5,7-18]. At room temperature, the alloy is comprised mostly α, but at the β transus temperature, around 980-996

°C [10], the β-phase becomes completely stable up to the melting point [19]. A rapid cooling rate from the homogeneous β produces martensitic α-phases [20]. However if there is a lower cooling rate below the β transus temperature, grain boundary α-phase may grow at the β-grain boundaries or a plate-like α structure may form within the prior β grains at lower temperatures [18]. The plate-like α structure is known as Widmanstätten.

Several studies have shown variation in microstructural development as a result of scan speed, beam voltage and current, cooling rates, etc. [12,21,22]. These variations in operational parameters have been suggested as the main cause for variations in mechanical properties. Some studies have shown that the mechanical properties of EBAM Ti-64 are comparable to those of conventional processes such as casting or wrought, while others have shown that EBAM Ti-64 results in an improved mechanical performance [7,23].

The work by Rao, et al. [13] utilized two (bead-over-bead, BoB) and three pass (bead-over-bead-over-bead, BoBoB) electron beam welding (EBW) techniques. These techniques were employed with the idea that when the weld metal is solidifying after the first pass with a preheated heat affected zone (HAZ), the second pass (called BoB) is run on the first pass with the benefit of the preheat effect from the prior weld passes. Because of the preheating effect, it was expected that the BoB technique should lead to a relatively slower cooling rate compared to conventional EBW. The low toughness observed in these welds are attributed to the faster cooling rate typically associated with conventional EBW. Overall, the study showed that the BoB and the BoBoB technique improved both notch toughness and fracture toughness of Ti-64 electron beam weld metals.

We found the BoBoB technique to be similar to what occurs in the EBAM process. Thus, the microstructures and properties that were observed in the work by Rao, et al. [13] were

compared to what we found in our study. Also, due to the preferential grain growth of the β phase in Ti-64, microstructure and microhardness were compared as a function of build direction (e.g., vertically and horizontally).

3.2 Experimental Materials and Procedures

In the present study, all Ti-64 EBAM samples were produced from powders at NASA Marshall Space Flight Center (MSFC) in Huntsville, Alabama using the Arcam S12 EBM system at an accelerating voltage of 60Kv, a beam current of 5mA, and a scanning speed of 200 mm/s. We were given a sample of the powders used and they were imaged using scanning electron microscopy (SEM) and measured to find a size distribution. The initial EBAM specimen we were given to test was a bar. Although no information was given with respect to build direction, it is believed that the build direction is horizontal. The EBAM bar and a wrought Ti-64 rod were arbitrarily sectioned to obtain views of the cross-section and transverse for OM.

The samples were prepared using standard metallographic procedures, including grinding up to 800 grit SiC papers, and polished using diamond suspension to 0.05μm. The samples were etched in Kroll's reagent (2ml HF, 6ml HNO_3, 92ml water) for 30 s. The surface and transverse views were used for Vickers microhardness testing at 500 grams force for 15 seconds. The resulting values were compared to those for the wrought sample. The first round of microhardness testing were in random areas of the sample in order to get results comparable to those found in literature. The second round of testing was done in a straight line, from one

arbitrary end of the sample to the opposite end. Therefore, the "distance" axis on Figure 3.3 shows a distance interval between indentions.

3.3 Results and Discussion

A sample of the starting powders that were used to make the EBAM specimens was obtained. They were measured via a single SEM image and found to range in size from 5μm to 109μm with the majority of the powders falling in the range of 50μm-89μm. The powders and the size distributions are shown in Figure 3.1.

The first EBAM Ti-64 specimen obtained was a bar that measured just below 14 cm in length. No information about this specimen was given with respect to build direction, however upon visual examination, the sample seems to have been built horizontally. A photograph of the specimen is shown in Figure 3.2. This specimen was arbitrarily cut to obtain cross sectional and transversal views. In the schematic shown in Figure 3.3, the cross section is the vertical line and the transverse is the horizontal line. Cross section is viewed from the right to the left into sample 2, while transverse is viewed from the bottom to the top into sample 1.

It is typical of Ti-64 samples from EBAM to show an ordered lamellar structure consisting of fine grains. This is a result of the EBAM processing characteristics (i.e. small melt pool and rapid cooling) [8,13,17,24-29]. The phases of EBAM Ti-64 samples include some α phase at the β grain boundaries, which is finer than that obtained by wrought or metal casting as shown by Facchini et al.[8]. Koike et al. [27] compared the EBAM Ti-64 microstructures to counterparts from cast and wrought Ti-64 specimens. The microstructure of the wrought Ti-6Al-4V specimen consisted of slightly elongated α grains and intergranular β grains which is a typical Ti-64 microstructure from heat treatment conditions. Figure 3.4 compares the microstructures of EBAM and wrought Ti-64 with views of the cross section and transverse respectively. The

microstructures in the current study were found to be in agreement with those found by other researchers. The wrought alloy shows α grains (light) and an intergranular β phase (dark). The EBAM sample predominantly contains the martensitic α phase. As stated previously, a rapid cooling produces martensitic α-phases; but if there is a slower cooling rate below the β transus temperature, grain boundary α-phase may grow at the β-grain boundaries or the plate-like Widmanstätten structure may form within the prior β grains at lower temperatures [18], the microstructural differences between wrought and EBAM Ti-64 can be seen in the optical micrographs and the SEM micrographs shown in Figures 3.4-3.7.

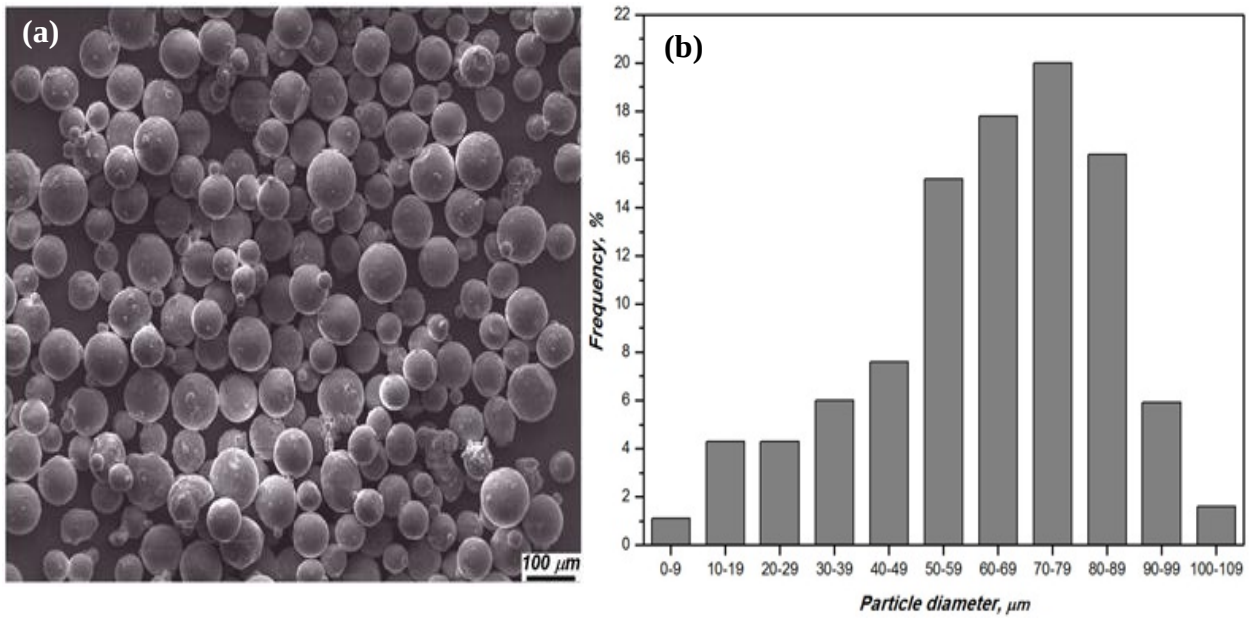

Figure 3.1 (a) Representative SEM Image of Ti-64 powders and (b) Graph showing the size distributions of the powders used to make specimens in this study.

Figure 3.2 EBAM Ti-64 specimen from NASA MSFC.

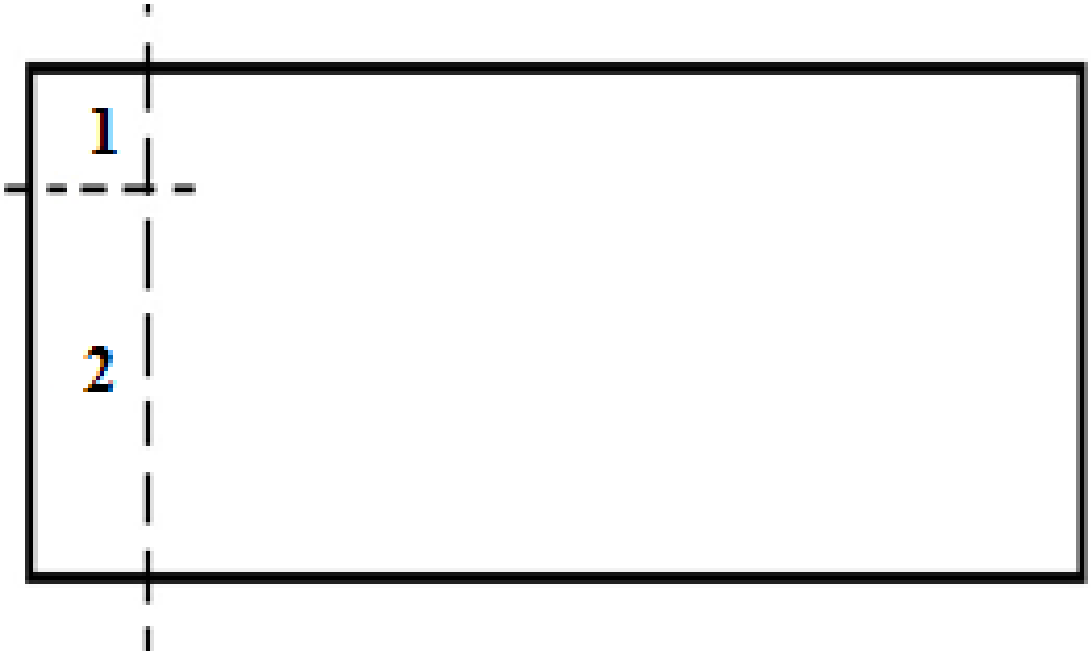

Figure 3.3 Schematic of cross section and transverse views of EBAM Ti-64.

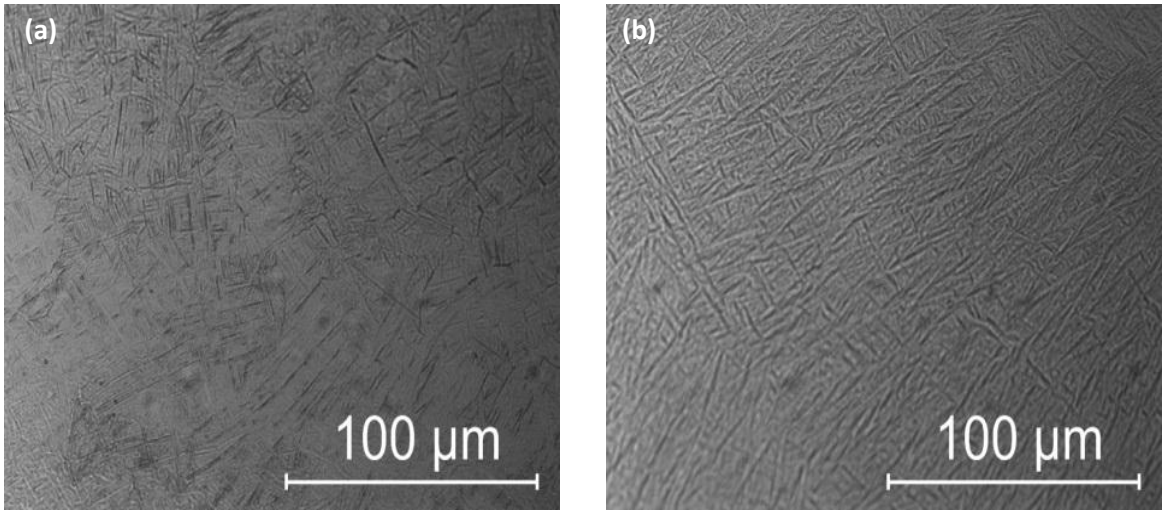

Figure 3.4 Light micrographs showing (a) cross section and (b) transverse of the EBAM Ti-64.

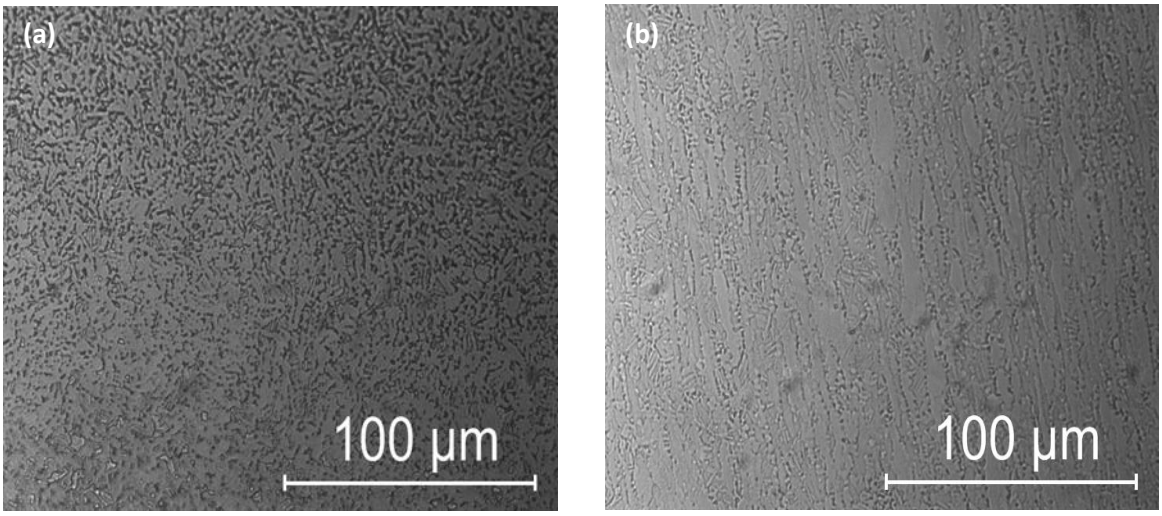

Figure 3.5 Light micrographs showing the (a) cross section and (b) transverse of wrought Ti-64

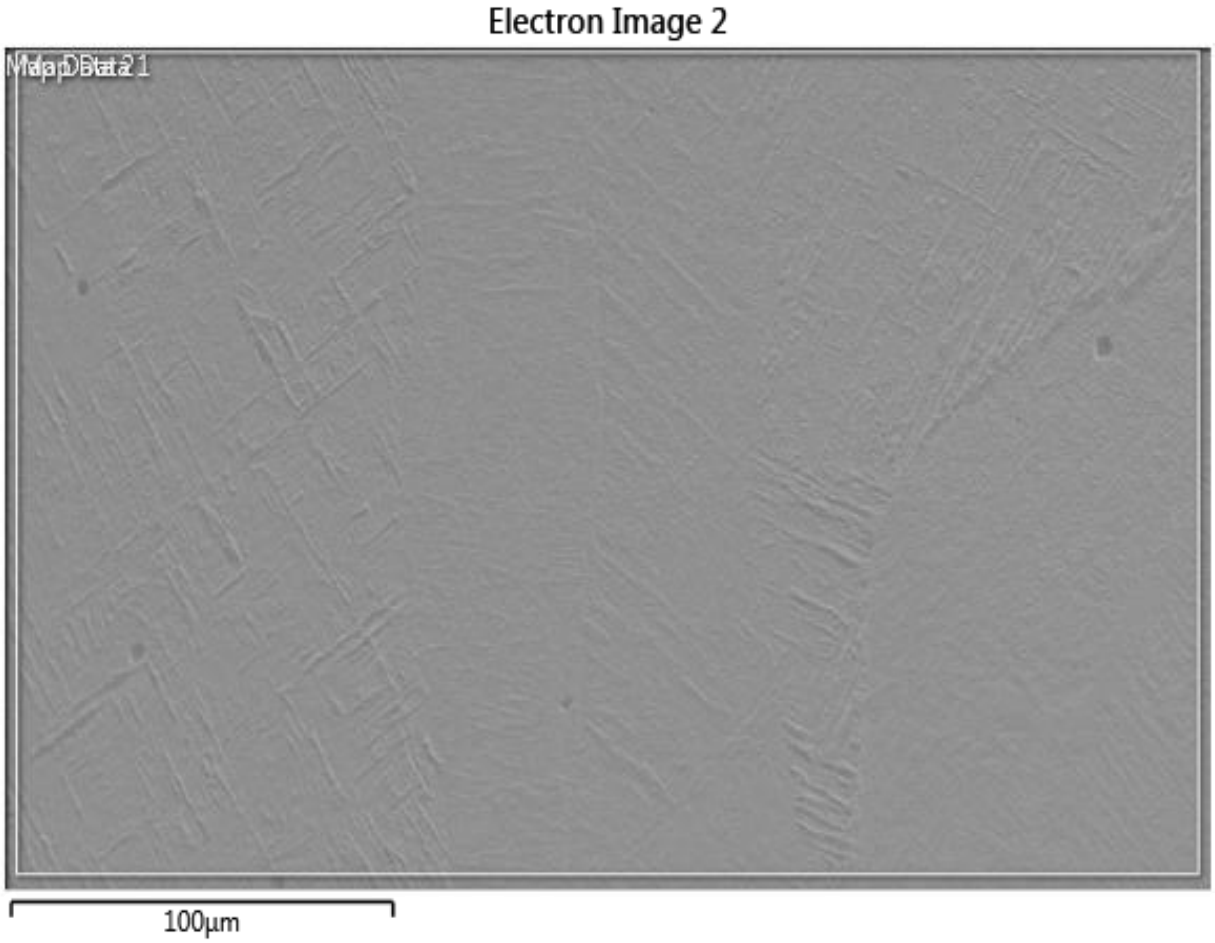

Figure 3.6 SEM image of EBAM Ti-64

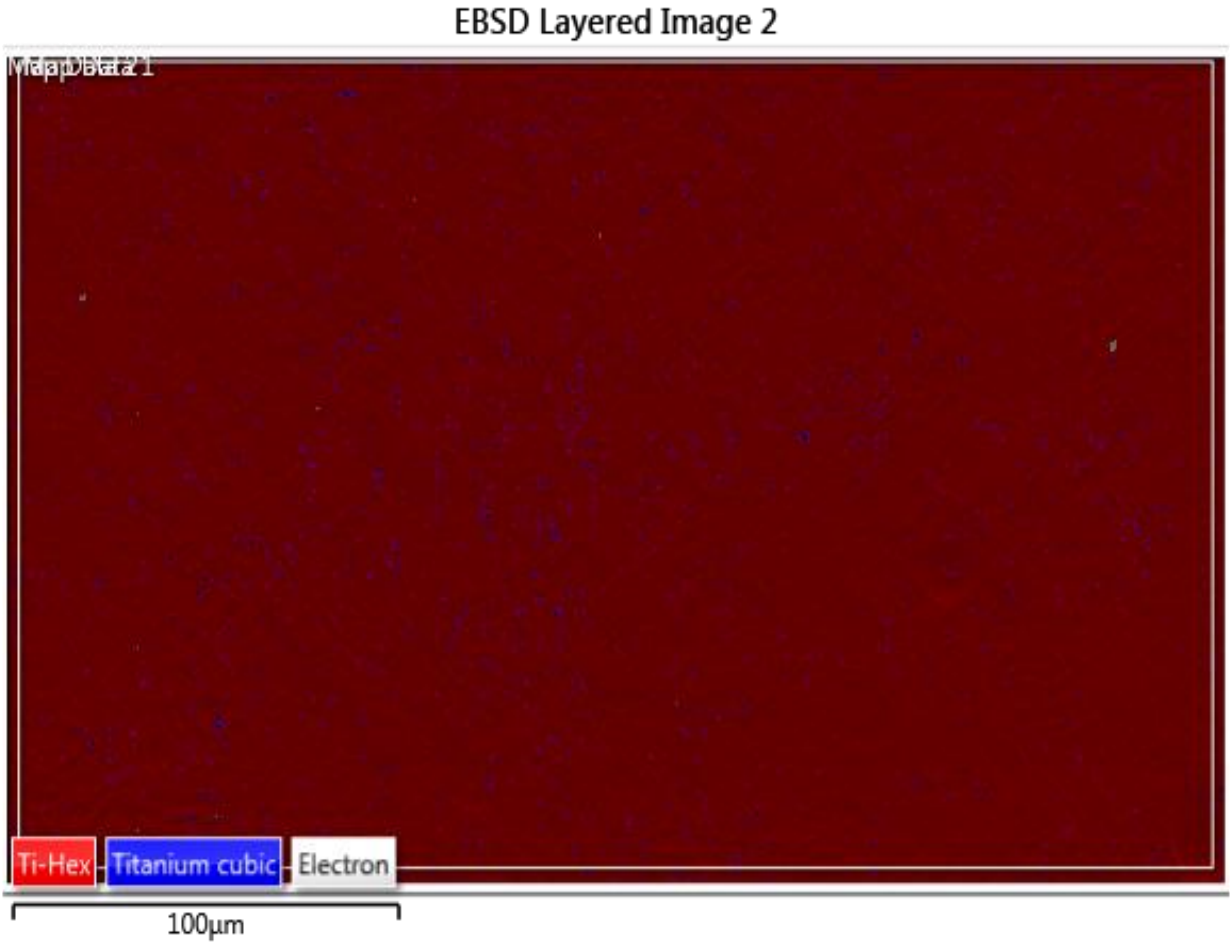

Figure 3.7 EBSD layered image of EBAM Ti-64 showing hexagonal and cubic phases present.

Some studies have indicated that mechanical properties of EBAM parts are comparable to those from conventional processes [17], however other studies have shown that mechanical properties, microhardness in particular, can be improved by the EBAM process [13,30]. The microstructures in the present study were found to be very similar to those reported by Rao et al. [13]. In their study, the fracture toughness of EBW Ti-64 was investigated. The EBW researchers reported microhardness at the HAZ that were nearly identical to the microhardness of the EBAM specimens in this study. The microstructures were identical because the process of EBW is very similar to the process by which the EBAM samples were made. They measured Vickers microhardness (HV) of a Stringer bead, then bead-over-bead (BoB), and bead-over-bead-over-bead (BoBoB). Since the three pass BoBoB welding process was found to be most similar to the EBAM processing in the present study, the results were compared to the microhardness values from Rao et al. shown in Table 3.1. Typical images showing indentations in the EBAM specimens for the present work are shown in Figure 3.8.

In the study by Rao et al., the researchers did not explicitly indicate where the microhardness measurements were taken on the specimens. For accurate comparison, the Vickers microhardness values obtained were taken in arbitrary areas of the sample where the Widmanstätten structure could be observed, as it is not seen throughout the entire sample. For the sake of comparison, Rao et al. reported an average of 341 HV for the wrought Ti-64.

Table 3.1 Microhardness values of Ti-64 EBAM specimens compared to EBW specimens in work by Rao, et al. [12].

EBAM Specimens		BoBoB EBW by Rao, et al.
Cross-Sectional	Transverse	386
406.6	404.1	386
404.1	372.3	412
364.2	369.4	341
435.3	368.6	362
370.8	363.5	321
Average = 396.2	Average = 375.6	Average = 368

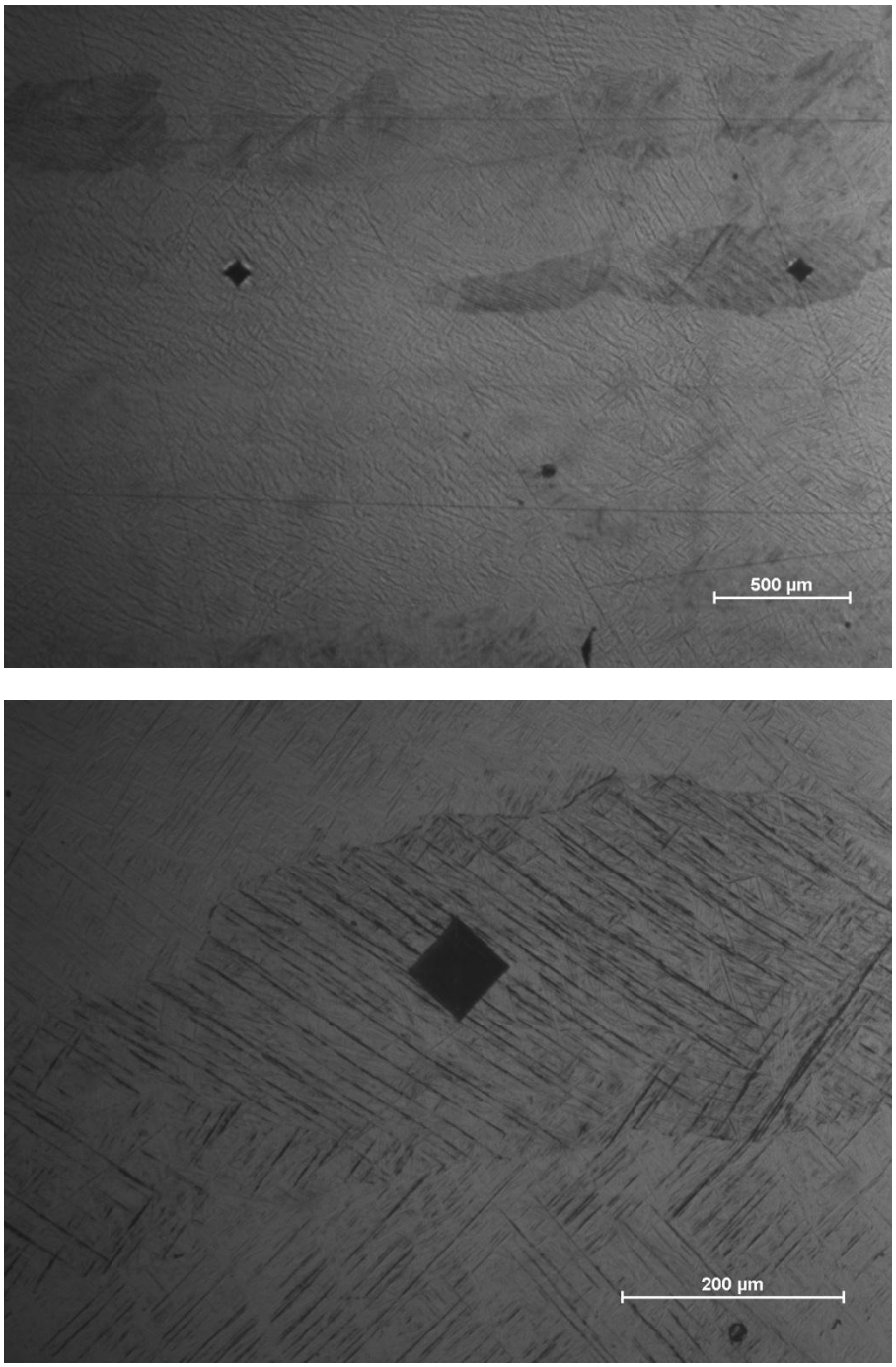

Figure 3.8 Typical microhardness indentations in the EBAM specimen.

To compare the EBAM samples with the wrought samples, Vickers microhardness testing was performed straight across the sample to include α′ rich areas of the sample as well as α′ deficient areas of the sample. The results are shown in Figure 3.9. The microhardness of the cross-sectional area of the EBAM Ti-64 sample was significantly harder than the wrought sample. There is no orientation effect causing a downward trend on the wrought Ti-64. The trend is merely coincidental as the hardness testing was performed across the diameter of the sample.

Per the work reported by Wang et al. [7], the EBW samples had higher HV than their rolled Ti-64 sample due to the presence of the α′ phase in the EBW sample. This singular phase is harder than both the α phase and the β phase present in the wrought sample. The hardness of the β phase is lower than that of the α phase, and the hardness of the martensitic α′ phase is higher than that the α phase. The microstructures in the present study are similar to those found by Wang et al. and this supports the fact that the EBAM sample consistently had significantly higher microhardness values than those of the wrought sample.

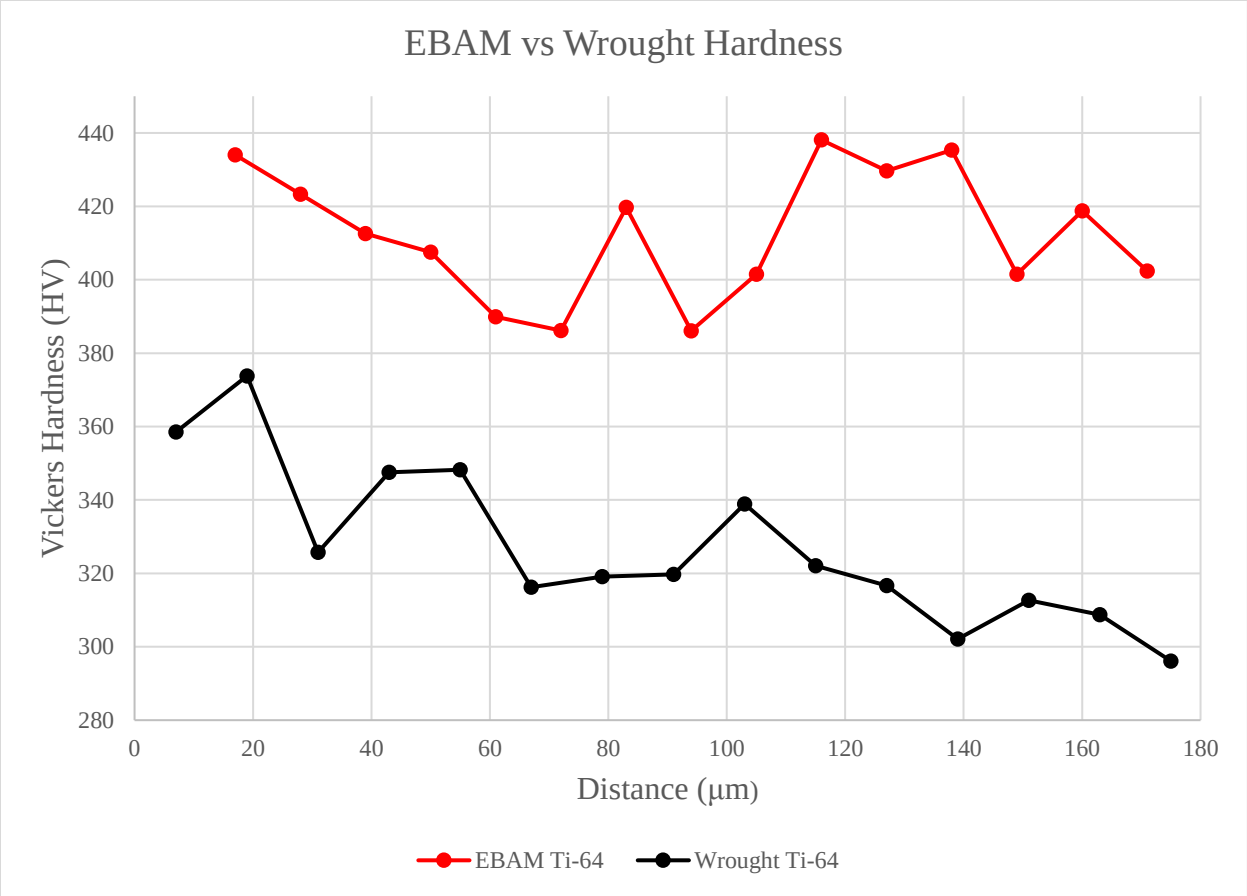

Figure 3.9 Microhardness comparison of EBAM Ti-64 vs Wrought Ti-64

3.4 Conclusions

In this paper, the microstructure and Vickers microhardness of EBAM Ti-64 and wrought Ti-64 were compared. The main conclusions include:

- The microstructures of the wrought sample expectedly showed α grains and an intergranular β phase. The EBAM microstructures showed the martensitic needle structure from within the prior β grains.
- The EBAM process increases the microhardness of Ti-64 compared to the wrought sample. This can be attributed to the formation of the α phase present in the EBAM samples which is harder compared to both the α and β phases present in the wrought Ti-64.

References

[1] W. E. Frazier, "Metal Additive Manufacturing: A Review," *Journal of Materials Engineering and Performance* 23 (2014) 1917-1928.

[2] V. Petrovic, J. Vicente Haro Gonzalez, O. Jordá Ferrando, J. Delgado Gordillo, J. Ramón Blasco Puchades and L. Portolés Griñan, "Additive layered manufacturing: sectors of industrial application shown through case studies," *International Journal of Production Research* 49 (2011) 1061-1079.

[3] S. Biamino, A. Penna, U. Ackelid, S. Sabbadini, O. Tassa, P. Fino, M. Pavese, P. Gennaro and C. Badini, "Electron beam melting of Ti–48Al–2Cr–2Nb alloy: Microstructure and mechanical properties investigation," *Intermetallics* 19 (2011) 776-781.

[4] L. E. Murr, S. M. Gaytan, D. A. Ramirez, E. Martinez, J. Hernandez, K. N. Amato, P. W. Shindo, F. R. Medina and R. B. Wicker, "Metal Fabrication by Additive Manufacturing Using Laser and Electron Beam Melting Technologies," *Journal of Materials Science & Technology* 28 (2012) 1-14.

[5] L. E. Murr, E. Martinez, K. N. Amato, S. M. Gaytan, J. Hernandez, D. A. Ramirez, P. W. Shindo, F. Medina and R. B. Wicker, "Fabrication of Metal and Alloy Components by Additive Manufacturing: Examples of 3D Materials Science," *Journal of Materials Research and Technology* 1 (2012) 42-54.

[6] R. R. Boyer, "An Overview on the Use of Titanium in the Aerospace Industry," *Materials Science and Engineering: A* 213 (1996) 103-114.

[7] S. Wang and X. Wu, "Investigation on the microstructure and mechanical properties of Ti–6Al–4V alloy joints with electron beam welding," *Materials & Design* 36 (2012) 663-670.

[8] L. Facchini, E. Magalini, P. Robotti and A. Molinari, "Microstructure and mechanical properties of Ti-6Al-4V produced by electron beam melting of pre-alloyed powders," *Rapid Prototyping Journal* 15 (2009) 171-178.

[9] C. Charles, "Modelling microstructure evolution of weld deposited Ti-6Al-4V," *Thesis, Luleå University of Technology* (2008).

[10] R. Ding, Z. X. Guo and A. Wilson, "Microstructural Evolution of a Ti–6Al–4V Alloy During Thermomechanical Processing," *Materials Science and Engineering: A* 327 (2002) 233-245.

[11] J. Karlsson, A. Snis, H. Engqvist and J. Lausmaa, "Characterization and comparison of materials produced by Electron Beam Melting (EBM) of two different Ti–6Al–4V powder fractions," *Journal of Materials Processing Technology* 213 (2013) 2109-2118.

[12] N. Hrabe and T. Quinn, "Effects of processing on microstructure and mechanical properties of a titanium alloy (Ti–6Al–4V) fabricated using electron beam melting (EBM), part 1: Distance from build plate and part size," *Materials Science and Engineering: A* 573 (2013) 264-270.

[13] K. P. Rao, K. Angamuthu and P. B. Srinivasan, "Fracture toughness of electron beam welded Ti6Al4V," *Journal of Materials Processing Technology* 199 (2008) 185-192.

[14] A. Majorell, S. Srivatsa and R. R. Picu, "Mechanical Behavior of Ti-6Al-4V at High and Moderate Temperatures," *Materials Science and Engineering: A* 326 (2002) 297 297-305.

[15] J. Parthasarathy, B. Starly, S. Raman and A. Christensen, "Mechanical evaluation of porous titanium (Ti6Al4V) structures with electron beam melting (EBM)," *Journal of the mechanical behavior of biomedical materials* 3 (2010) 249-259.

[16] Y. Zhai, H. Galarraga and D. A. Lados, "Microstructure Evolution, Tensile Properties, and Fatigue Damage Mechanisms in Ti-6Al-4V Alloys Fabricated by Two Additive Manufacturing Techniques," *Procedia Engineering* 114 (2015) 658-666.

[17] L. E. Murr, E. V. Esquivel, S. A. Quinones, S. M. Gaytan, M. I. Lopez, E. Y. Martinez, F. Medina, D. H. Hernandez, E. Martinez, J. L. Martinez, S. W. Stafford, D. K. Brown, T. Hoppe, W. Meyers, U. Lindhe and R. B. Wicker, "Microstructures and mechanical properties of electron beam-rapid manufactured Ti–6Al–4V biomedical prototypes compared to wrought Ti–6Al–4V," *Materials Characterization* 60 (2009) 96-105.

[18] C. C. Murgau, R. Pederson and L. E. Lindgren, "A model for Ti–6Al–4V microstructure evolution for arbitrary temperature changes," *Modelling and Simulation in Materials Science and Engineering* 20 (2012) 055006.

[19] S. Roy and S. Suwas, "Effect of Hypoeutectic Boron Addition on the beta Transus of Ti6Al4V Alloy," *Metallurgical and Materials Transactions A* 42A (2011) 2535-2541.

[20] T. Ahmed and H. J. Rack, "Phase transformations during cooling in a b titanium alloys." (1998). 243

[21] X. Gong, J. Lydon, K. Cooper and K. Chou, "Beam speed effects on Ti–6Al–4V microstructures in electron beam additive manufacturing," *Journal of Materials Research* 29 (2014) 1951-1959.

[22] A. Dehghan-Manshadi, M. H. Reid and R. J. Dippenaar, "Effect of microstructural morphology on the mechanical properties of titanium alloys," *Journal of Physics: Conference Series* 240 (2010) 012022.

[23] M. Shunmugavel, A. Polishetty and G. Littlefair, "Microstructure and mechanical properties of wrought and additive manufactured Ti-6Al-4V cylindrical bars," *Procedia Technology* 20 (2015) 231-236.

[24] C. de Formanoir, S. Michotte, O. Rigo, L. Germain and S. Godet, "Electron beam melted Ti–6Al–4V: Microstructure, texture and mechanical behavior of the as-built and heat-treated material," *Materials Science and Engineering: A* 652 (2016) 105-119.

[25] X. Gong, T. Anderson and K. Chou, "Review on powder-based electron beam additive manufacturing technology," *Manufacturing Review* 1 (2014) 2.

[26] O. L. A. Harrysson, O. Cansizoglu, D. J. Marcellin-Little, D. R. Cormier and H. A. West, "Direct metal fabrication of titanium implants with tailored materials and mechanical properties using electron beam melting technology," *Materials Science and Engineering: C* 28 (2008) 366-373.

[27] M. Koike, K. Martinez, L. Guo, G. Chahine, R. Kovacevic and T. Okabe, "Evaluation of titanium alloy fabricated using electron beam melting system for dental applications," *Journal of Materials Processing Technology* 211 (2011) 1400-1408.

[28] S. Yoon, R. Ueji and H. Fujii, "Microstructure and texture distribution of Ti–6Al–4V alloy joints friction stir welded below β-transus temperature," *Journal of Materials Processing Technology* 229 (2016) 390-397.

[29] L. E. Murr, S. A. Quinones, S. M. Gaytan, M. I. Lopez, A. Rodela, E. Y. Martinez, D. H. Hernandez, E. Martinez, F. Medina and R. B. Wicker, "Microstructure and mechanical behavior of Ti-6Al-4V produced by rapid-layer manufacturing, for biomedical applications," *Journal of the mechanical behavior of biomedical materials* 2 (2009) 20-32.

[30] S. M. Gaytan, L. E. Murr, E. Martinez, J. L. Martinez, B. I. Machado, D. A. Ramirez, F. Medina, S. Collins and R. B. Wicker, "Comparison of Microstructures and Mechanical Properties for Solid and Mesh Cobalt-Base Alloy Prototypes Fabricated by Electron Beam Melting," *Metallurgical and Materials Transactions A* 41 (2010) 3216-3227.

CHAPTER 4

PREFERENTIAL GROWTH OF THE B-PHASE IN TI-6AL-4V AS A FUNCTION OF BUILD DIRECTION FOR COMPONENTS MADE BY ELECTRON BEAM ADDITIVE MANUFACTURING

Abstract

Electron Beam Additive Manufacturing (EBAM) is a relatively new additive manufacturing (AM) technology that uses a high-energy electron beam to melt and fuse powders to build full-density parts in a layer by layer fashion. EBAM can fabricate metallic components, particularly, of complex shapes, in an efficient and cost-effective manner compared to conventional manufacturing means. EBAM is an enabling technology for rapid manufacturing (RM) of metallic components, and thus, can efficiently integrate the design and manufacturing of aerospace components. However, EBAM for aerospace-related applications remain limited because the effect of the EBAM process on part characteristics is not fully understood. In this study, the preferential growth of the β-phase of Ti-6Al-4V as a function of build direction for components made using EBAM was investigated. The mechanical properties were compared to those for wrought Ti-6Al-4V.

4.1 Introduction

Ti-6Al-4V (Ti-64) is the most widely used titanium alloy in the aerospace industry due to its versatile combination of mechanical properties in its wrought processed form [1-3]. Ti-64 consists of allotropic phases: the body centered cubic (BCC) β-phase that is stabilized by the 4% vanadium, and the hexagonal close-packed (HCP) structured α-phase that is stabilized by the 6% aluminum [4]. At room temperature the alloy mostly consists of the α-phase, but when it is heated to the β transus temperature around 980-996 °C, the β-phase becomes completely stable up to the melting point [5,6]. A rapid cooling rate, i.e. above 137 °C/s [7,8], from the homogenous β-phase produces martensitic α-phases.

Electron beam additive manufacturing (EBAM) is a relatively new additive manufacturing (AM) technique that utilizes an electron beam to melt and fuse powders in order to build full density parts in a layer-by-layer fashion [9-13]. It is well known that the morphology of microstructure depends on processing, and wrought Ti-64 is well understood, however it is not fully understood what effect the EBAM process has on component characteristics. While there are many studies being conducted to investigate EBAM part characteristics, there is very little literature of x-ray diffraction (XRD) data of EBAM Ti-64 [14]. Furthermore there is no literature that shows a direct comparison of XRD spectra of EBAM Ti-64 to conventionally-processed wrought Ti-64. Previous work has shown that when subjected to a process such as electron beam welding (EBW), the hardness and fracture toughness of Ti-64 is increased [4,15]. However, there is no literature that directly addresses this phenomenon with respect to phase distribution in different build directions of EBAM Ti-64 and directly compare the results to wrought Ti-64. The main focus of this study is to investigate how the EBAM processing of Ti-64 components made by EBAM affects the growth of the β-phase with respect to build direction

and compare the mechanical properties of the resultant microstructures. This study also investigated the tensile-tested fracture surfaces of EBAM processed Ti-64.

4.2 Experimental Materials and Procedures

For this work, all Ti-64 EBAM samples were produced from powders at Marshall Space Flight Center (MSFC) in Huntsville, Alabama using the Arcam S12 EBM system at an accelerating voltage of 60Kv, a beam current of 5mA, and a scanning speed of 200 mm/s. After obtaining samples with specified build directions (e.g. vertical and horizontal), it was possible to make comparisons between the EBAM specimens with respect to build direction and then compare those differences to what was observed in the wrought specimen. For convention, Figure 4.1 shows a schematic of vertical and horizontal specimens and terminology that will be used to convey orientation: scanning direction (SD), transversal direction (TD), and building direction (BD).

A Hysitron® TriboIndenter with a three-side Berkovich diamond tip was used to determine hardness (GPa) and elastic modulus. The load as a function of time is shown in Figure 4.2. The Vickers hardness (HV) was performed on a Buehler Micromet 2004 microhardness tester under a load of 150 gf with the load time 10 s. Each average hardness value was averaged and obtained from fifteen measurements across the lateral direction in a 20 μm step. The estimated yield strength (σ_{YS}) was obtained through an empirical equation, which is widely accepted for hard materials without significant work-hardening behavior according to the literature [16-18]. Rockwell hardness was measured using a Wilson® hardness tester with a C-scale indenter (HRC). The major load was 150 kgf and the minor load was 10 kgf respectively. The chemical and characteristic spectrum analysis were carried out by utilizing an X-ray diffractometer (Bruker® AXS-D8 Discover, Co Kα radiation, λ_{Co}= 1.7889).

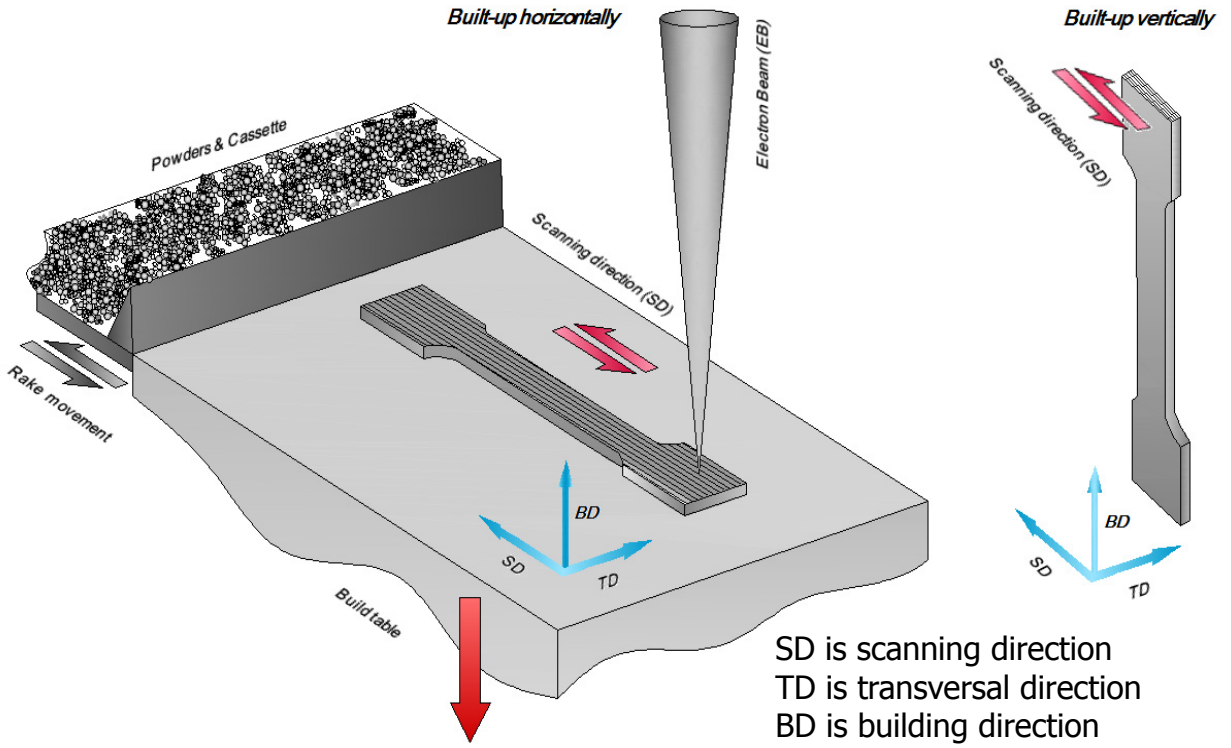

Figure 4.1 Schematic of S12 Arcam EBAM machine at NASA MSFC.

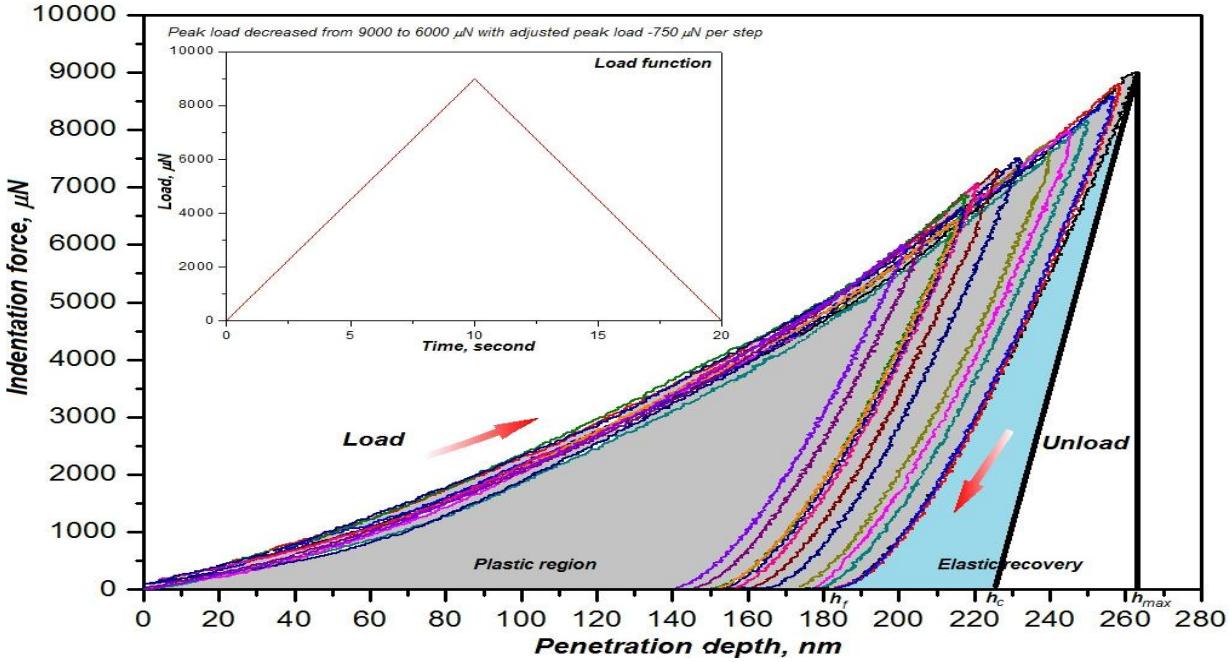

Figure 4.2 Nano indentation results with load function shown.

4.3 Results and Discussion

Microstructure

The morphology of the horizontal build EBAM Ti-64 specimen can be seen in Figure 4.3. The horizontal EBAM specimen exhibited a diffusionless transformation due to the high cooling rate. The transformation is realized by a martensitic transformation as $\beta \rightarrow \alpha'$ in according to the acicular α' from β within the columnar structure. The vertical build EBAM Ti-64 specimen is shown in Figure 4.4. The vertical EBAM specimen showed diffusional transformation. The Widmanstätten plates nucleated preferentially at the prior β grains forming a basket-weave morphology.

X-ray Diffraction

XRD was first performed on the wrought sample and a sample of the unmelted powder stock that was used to process the specimens used in this study. The specimens were not rotated during any data collection. Figure 4.5 shows the comparison of the powders and wrought sample. In the spectra for the wrought Ti-64, both α and β peaks are resolved and the indexed peaks are in agreement with what is found in literature [4,14,19]. It is worth noting that the β peaks in the powder are either not as strong or not as clearly resolved as the corresponding peaks in the wrought specimen.

Initially, for the samples that tested without respect to build direction, the spectra were in agreement with what was found in other reported works as it pertains to the α-peaks but we were unable to resolve any of the β-peaks that were found in literature unless the sample was oriented different ways. Figures 4.6 and 4.4 show the respective spectra for the horizontal and vertical built samples. The β peaks are more defined for the vertical build compared to the horizontal build.

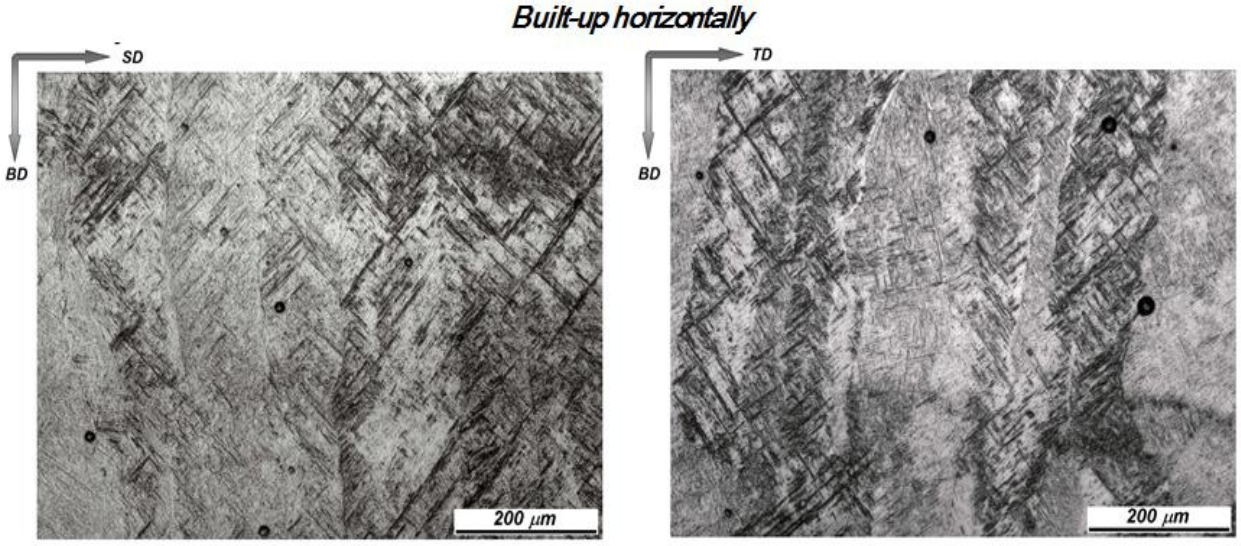

Figure 4.4 Morphology of the horizontal build EBAM Ti-64 specimen.

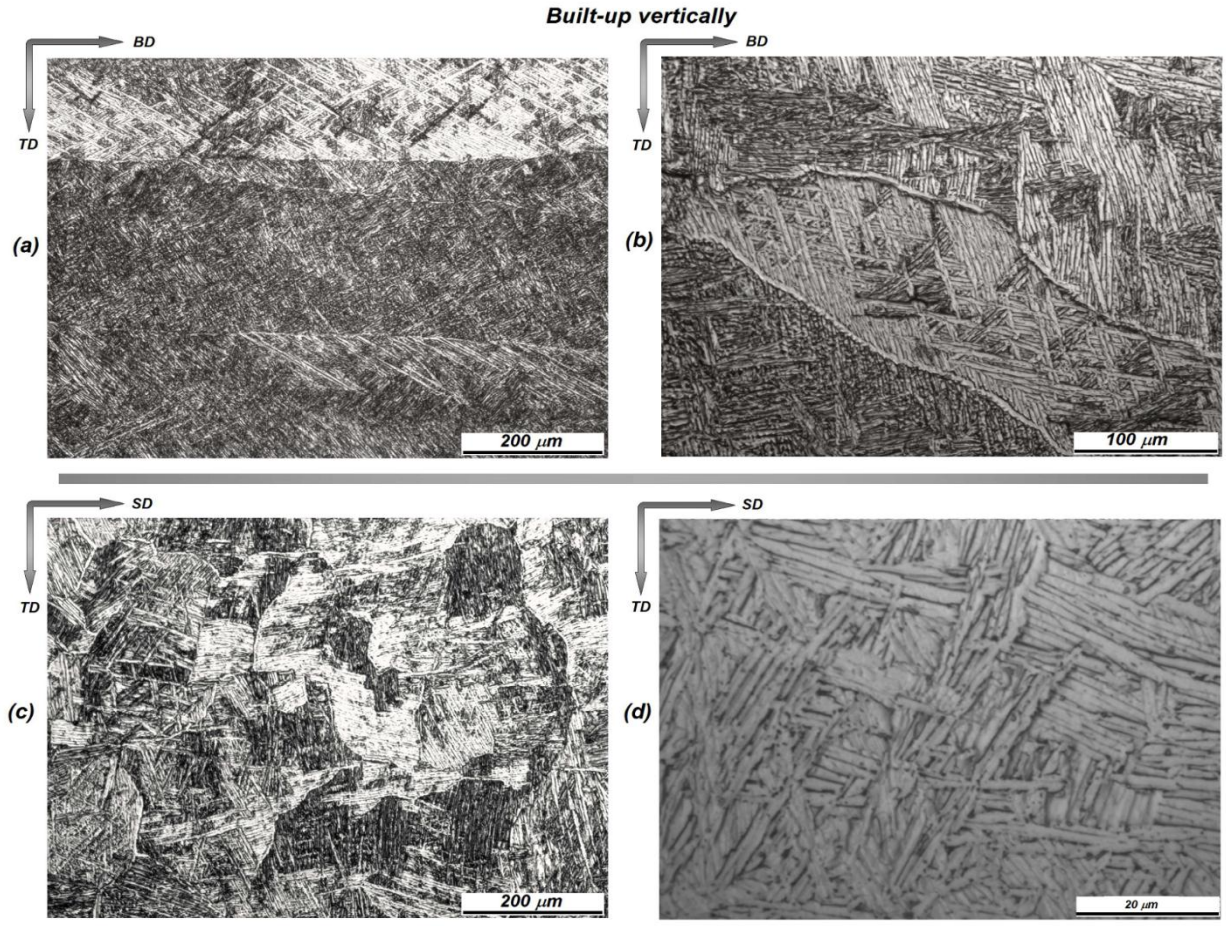

Figure 3.4 Morphology of the vertical build EBAM Ti-64 specimen.

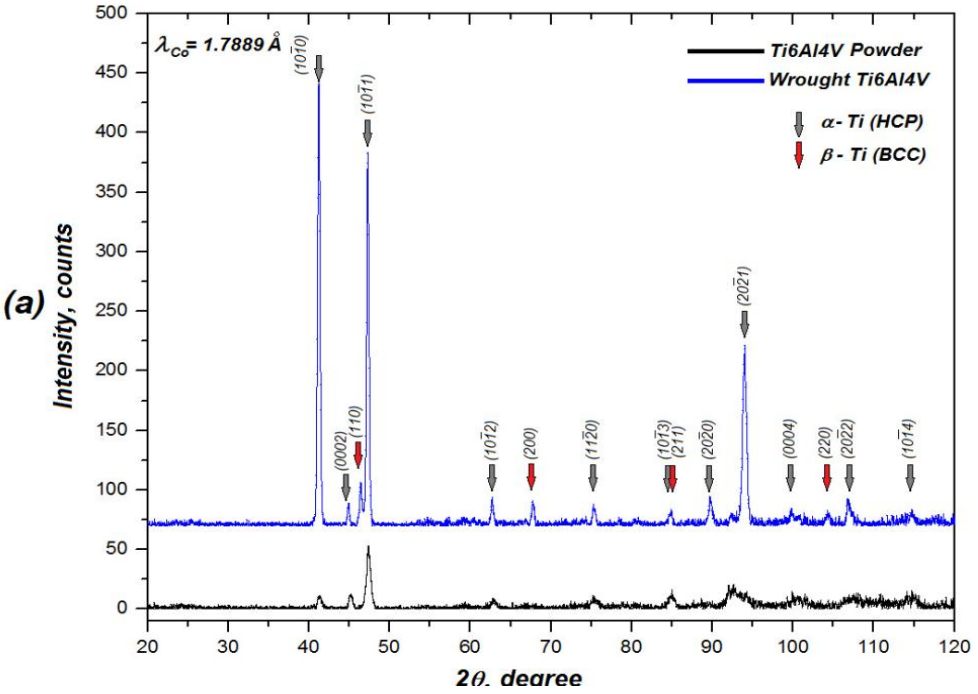

Figure 4.5 XRD comparison of wrought Ti-64 and unmelted Ti-64 powders.

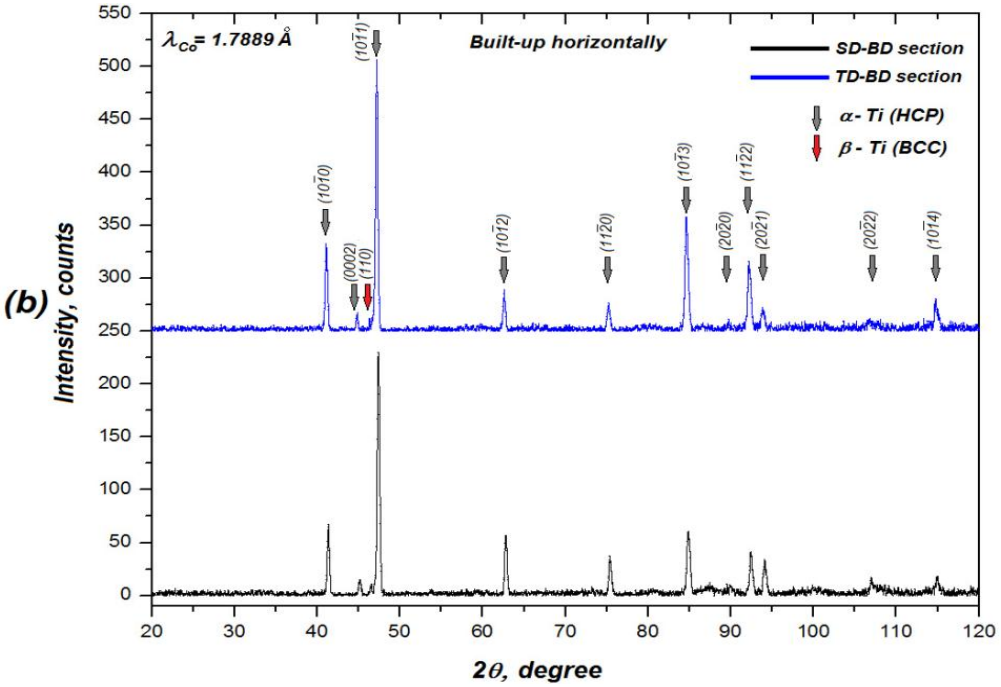

Figure 4.6 XRD spectra of the two sections of the horizontal build with α and β peaks identified.

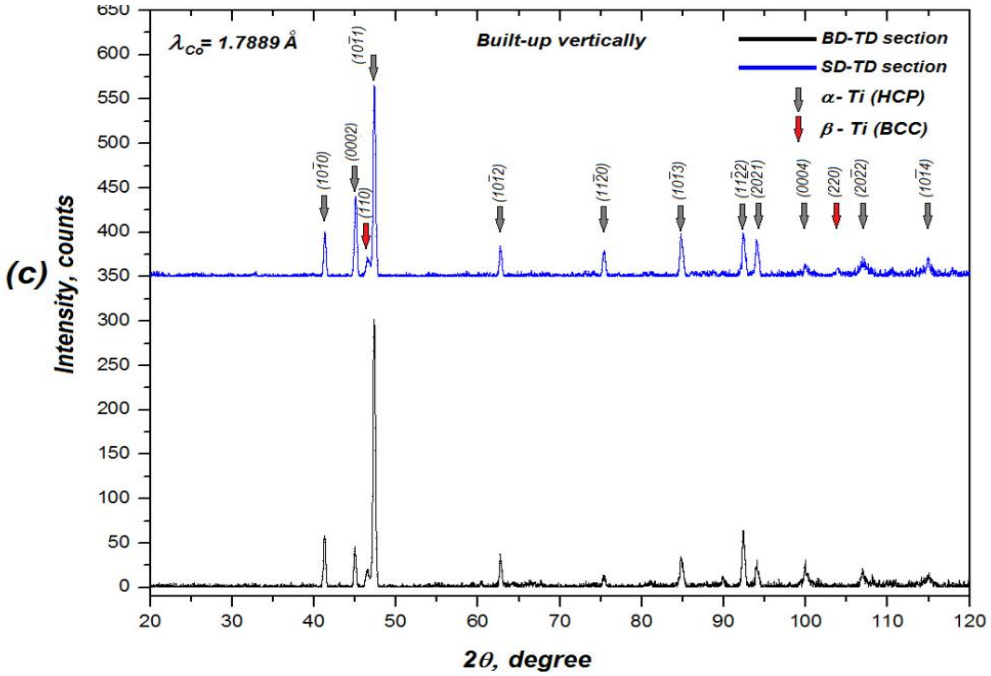

Figure 4.7 XRD spectra of the two sections of the vertical build with α and β peaks identified.

The β peaks were more resolved in some directions of both samples but not all. This suggests that there are differing amounts of the β-phase present between the build directions. Therefore, preferential growth direction for the β-phase occurs as a function of build direction. Figure 4.8 shows a β-phase distribution chart that is in agreement with what was observed in the XRD spectra. There was more of the β-phase present in the vertical build sample than in the horizontal build. Both EBAM build directions had less β-phase than the wrought sample.

Because of the difference in the amount of β in build directions it was expected that there would be a difference in hardness between the two build directions. As noted in the literature, the hardness of the β-phase tends to be lower than that of the α-phase [15]. Therefore nanoindentation testing was performed with respect to build direction. Table 4.1 shows the raw data obtained from hardness measurements with averages and standard deviation shown. Figures 4.9 - 4.11 show the hardness values and other mechanical properties from Table 4.1 graphically. Figure 4.9 shows average Vickers hardness along with corresponding estimated yield strength. As expected because of the differing amounts of the β-phase present in the different builds, the horizontal build EBAM specimen exhibited a higher hardness and yield strength than the vertical build specimen while they are both higher than the wrought specimen. Figure 4.10 shows the average hardness and corresponding elastic modulus and Figure 4.11 shows the average Rockwell Hardness C (HRC). Again, the horizontal EBAM build had higher values than the vertical EBAM build and both EBAM build directions were higher than the wrought.

Table 4.1 Experimental hardness data of Ti-64.

	Horiz. EBAM SD-BD	Horiz. EBAM TD-BD	Vert. EBAM BD-TD	Vert. EBAM SD-TD	Wrought
	414	403	364	359	337
	410	410	370	352	318
	406	411	366	364	342
	411	384	356	362	341
	409	398	361	352	328
	412	408	356	353	338
	403	411	372	371	336
	408	409	363	367	334
	410	402	362	359	335
	402	411	345	349	343
	407	402	386	363	321
	406	399	378	367	322
	406	403	348	351	325
	414	397	371	364	330
	417	394	377	336	323
Average HV	409	402.8	365	357.93	331.53
ST. DEV	4.19	7.66	11.2	9.09	8.26
	Horiz. EBAM SD-BD	Horiz. EBAM TD-BD	Vert. EBAM BD-TD	Vert. EBAM SD-TD	Wrought
	43	39	39	37	36
	37	42	37	35	37
	37	40	34	36	36
	41	39	35	38	31
	42	37	36	35	36
Average HRC	40	39.4	36.2	36.2	35.2
ST. DEV	2.83	1.82	1.92	1.30	2.39

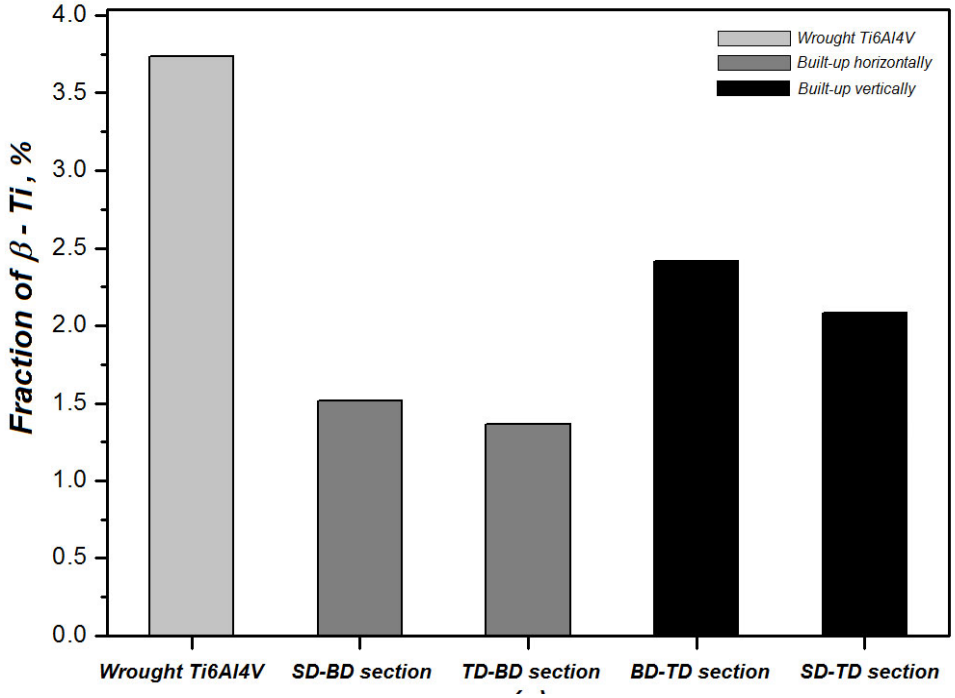

Figure 4.8 β-phase distribution chart comparing wrought Ti-64 to EBAM Ti-64.

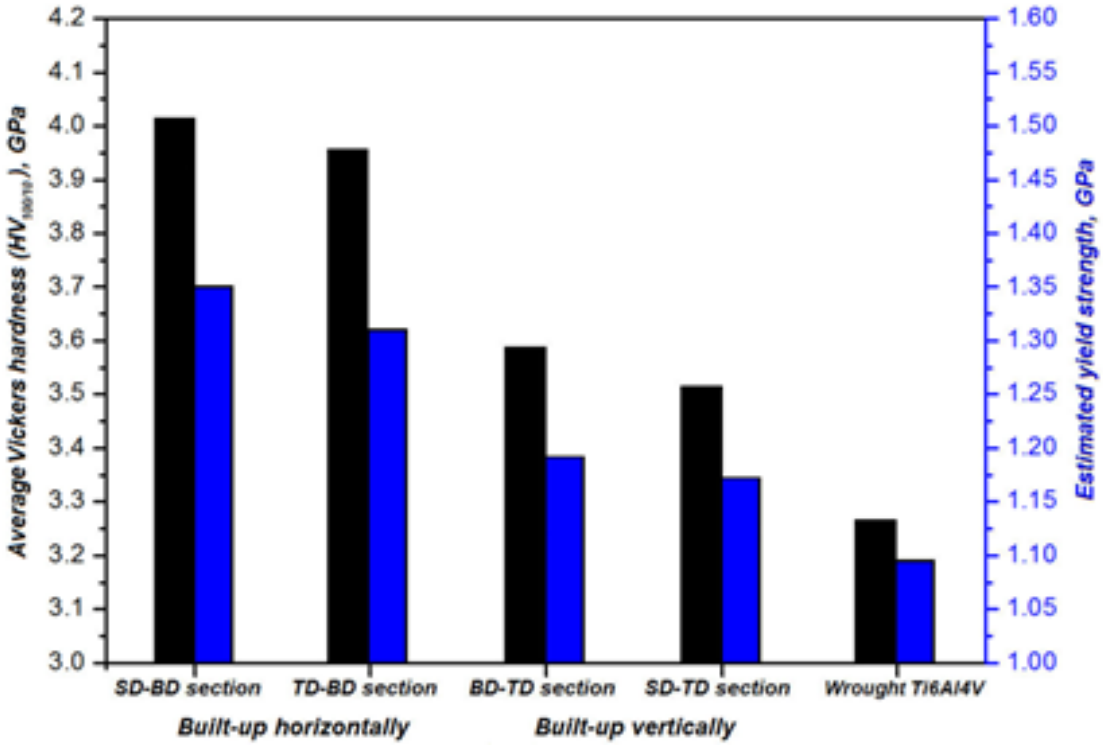

Figure 4.9 Average Vickers hardness and estimated yield strength of different orientations of EBAM and wrought Ti-64.

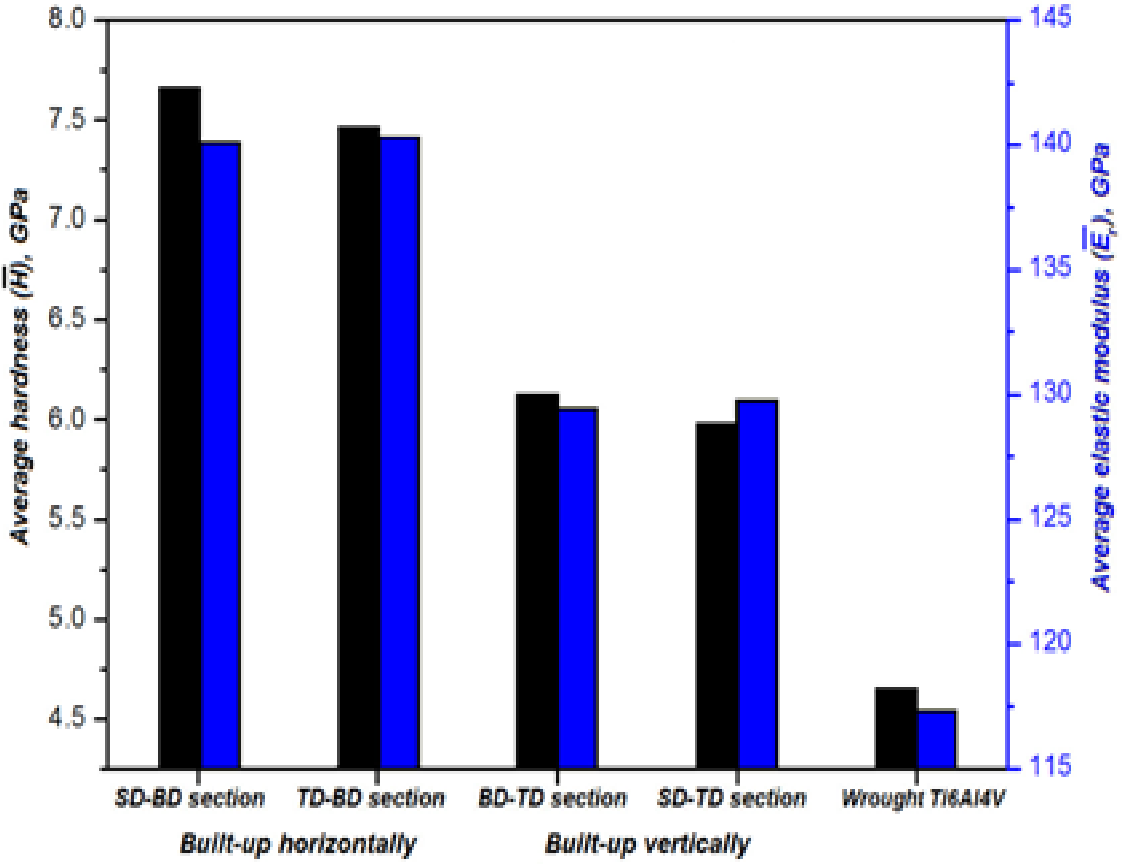

Figure 4.10 Average hardness and average elastic modulus of different orientations of EBAM and wrought Ti-64.

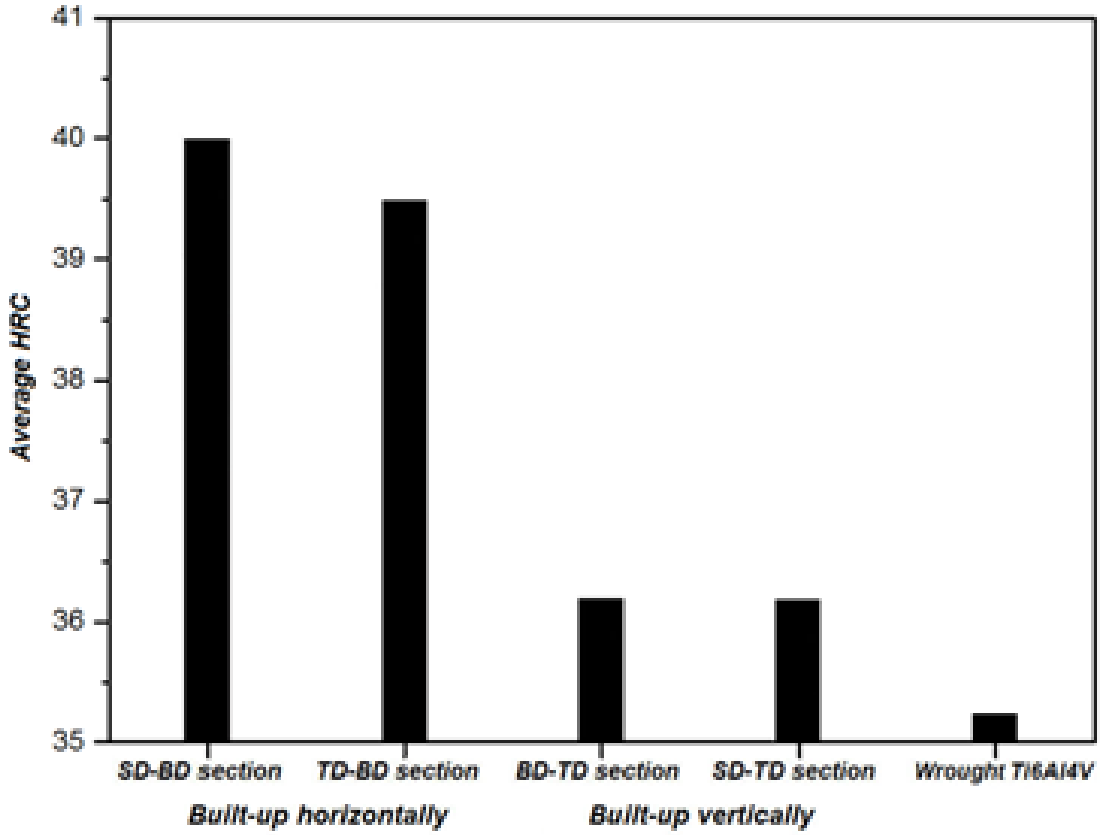

Figure 4.11 Average HRC of different orientations of EBAM and wrought Ti-64.

We can see that the hardness values of both EBAM samples are greater than that of the wrought sample. The difference in hardness values between the wrought and EBAM samples can be attributed to the presence of the martensitic α′ present in the EBAM samples [15]. The variation in hardness as a function of build direction was more significant in the horizontal sample due to less β present in the final microstructure.

Fracture Surfaces

Tensile test data is widely available for EBAM parts. Some studies [20] have shown that the UTS and ductility of wrought Ti-64 were higher than those of EBAM Ti-64. Others [21,22] have observed the opposite. Murr et al. [23] observed a higher yield strength and UTS in wrought Ti-64 and better ductility in EBAM parts. The difference in the data can likely be attributed to the nature of the powder recycling process of EBAM which can affect the oxygen content in the EBAM specimens. Koike et al. reported differences in build parameters can affect the final microstructure, porosity distribution, pore size, etc. and attributed this to rough specimen surfaces and possibly a higher oxygen content [20]. Table 4.2 below summarizes the tensile data of EBAM vs wrought Ti-64 from the literature. The experimental results of this study show higher values of hardness and yield strength than other researchers. A close relation to the yield strengths reported by Koike et al. [20] can be observed for the wrought and EBAM vertical build samples but the yield strength of the horizontal build EBAM is significantly higher than other reported values.

The fracture surfaces of both the EBAM build directions were examined via SEM. In the vertical sample, there was evidence of mostly brittle failure with some ductile failure. Failure appeared to occur along grain boundaries (figures 4.12 – 4.13). Figures 4.14 – 4.17 show the

fracture surfaces for the horizontal EBAM sample. The horizontal build also shows evidence of both ductile and brittle failures, with brittle being more prevalent.

Table 4.2 Reference Tensile data of EBAM and wrought Ti-64.

	YS (GPa)	UTS (GPa)	Ductility (%)	H (GPa)	Ref.
Wrought	0.735	0.775	2.3	3.619	[15]
	0.83	0.915	–	3.2	[16]
	1.10 – 1.15	1.15 – 1.20	16 – 25	3.8 – 4.1	[17]
EBAM	0.86	0.931	14	3.207	[15]
	0.79	0.87	–	–	[16]
	1.17 – 1.22	1.23 – 1.29	12 – 14	3.8 – 4.3	[17]

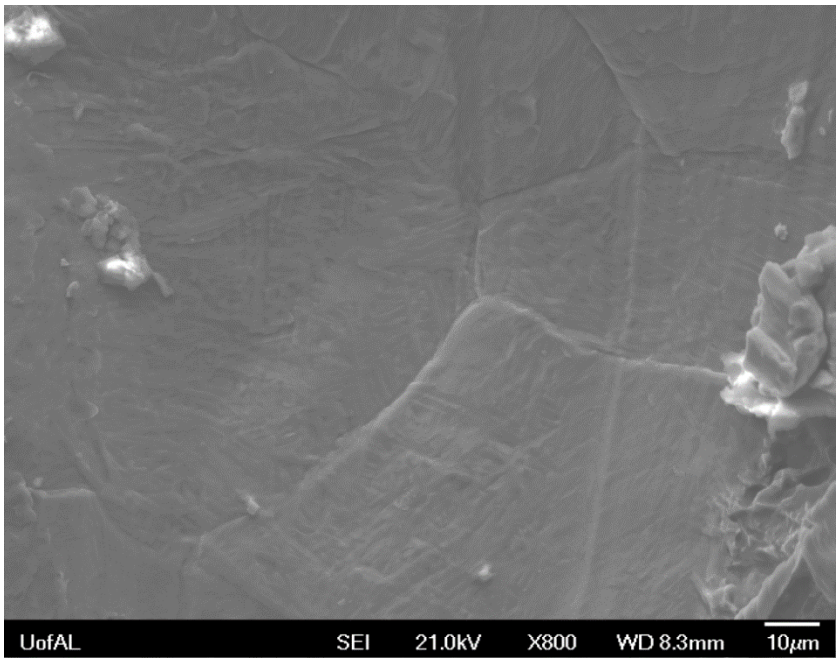

Figure 4.12 SEM image of vertical build EBAM fracture surface.

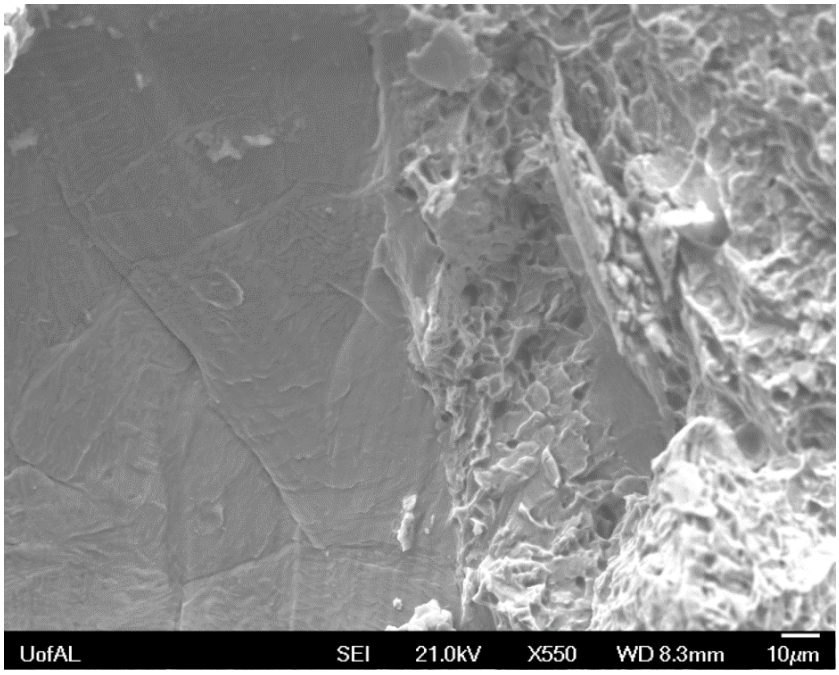

Figure 4.13 SEM image of vertical build EBAM fracture surface.

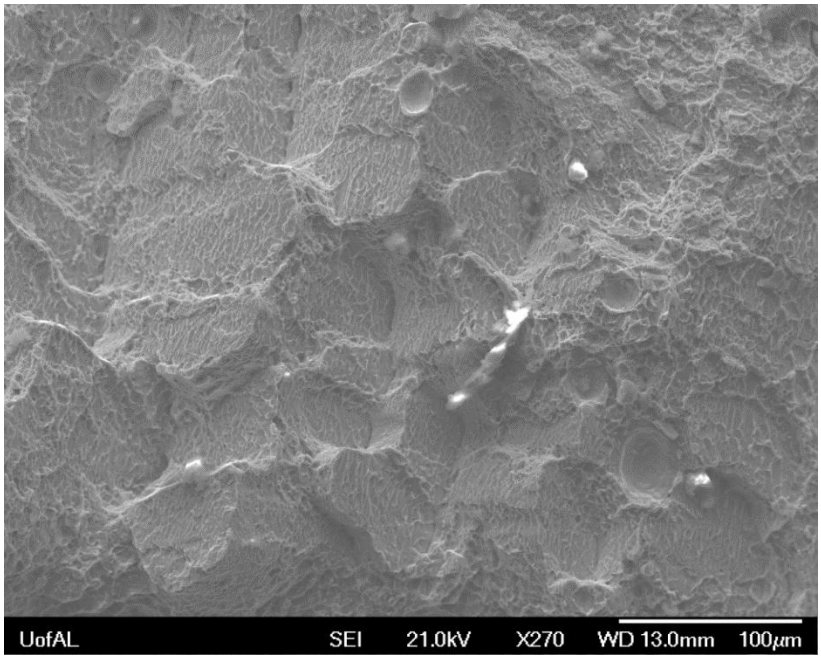

Figure 4.14 SEM image of horizontal build EBAM fracture surface.

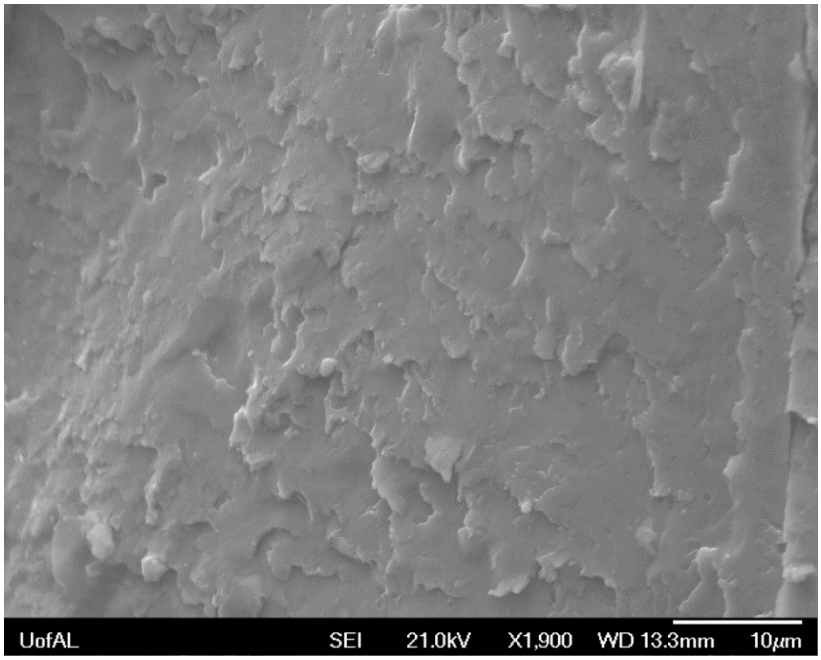

Figure 4.15 SEM image of horizontal build EBAM fracture surface.

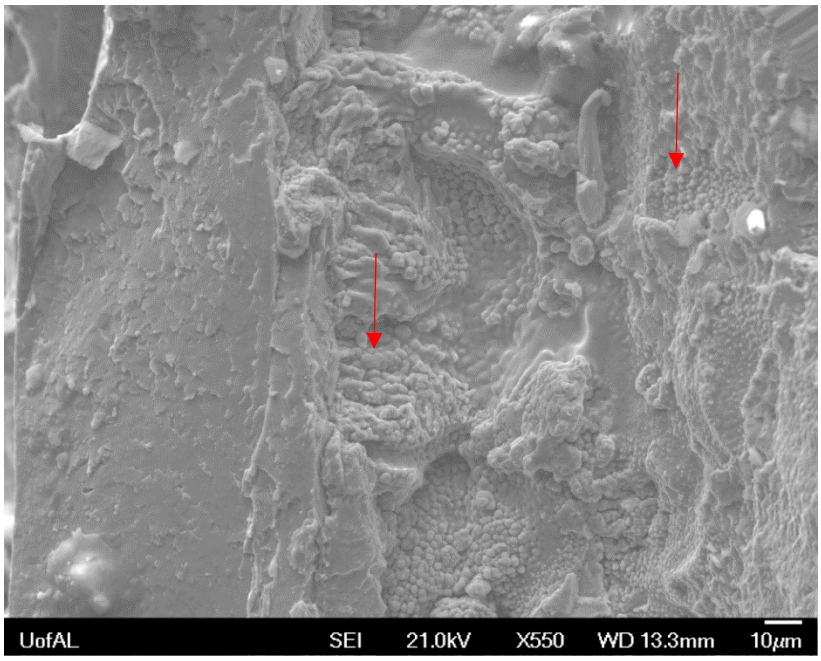

Figure 4.16 SEM image of horizontal build EBAM fracture surface.

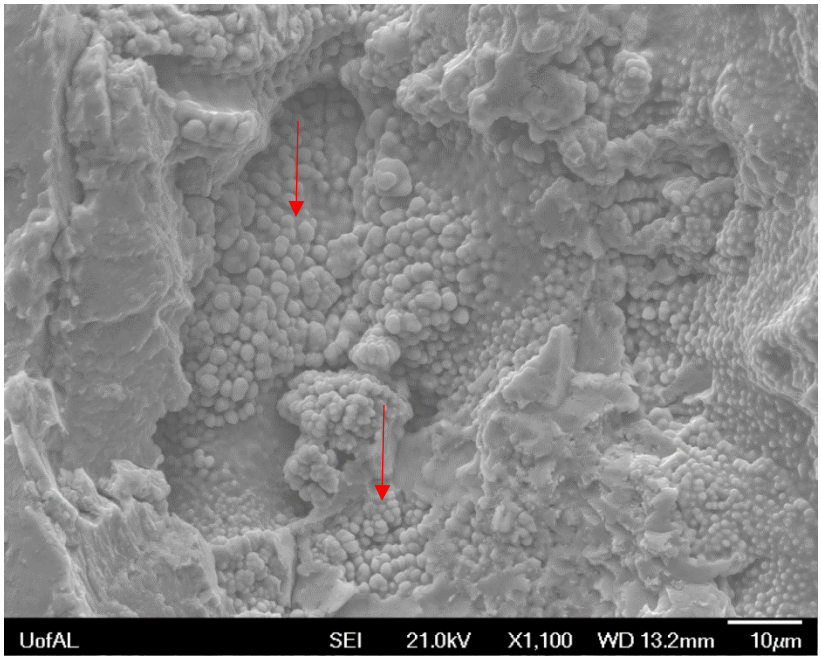

Figure 4.17 SEM image of horizontal build EBAM fracture surface.

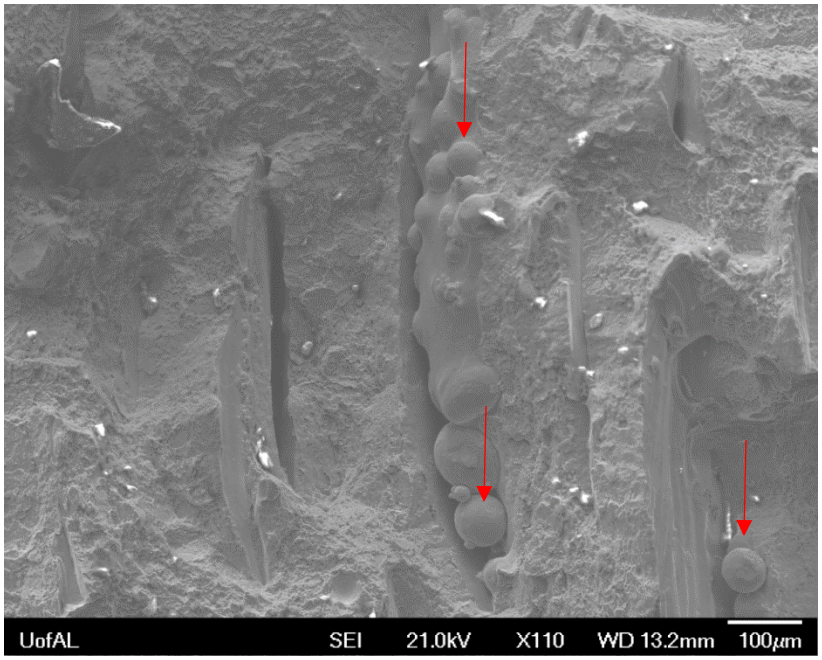

Figure 4.18 SEM image of horizontal build EBAM fracture surface.

In Figures 4.16-4.18 the regions denoted by arrows were initially thought to be unmelted powders on the fracture surface, however they are all far smaller than 10μm and this is impossible because our smallest powder size was 5μm. Due to the sizes of most of the defects being smaller than our largest stock powder size, it is believed that most of these regions are not unmelted powders, but instead are dendrites that formed in regions that did not solidify during the EBAM process. This is consistent with previous research on Ti alloys by Howell and Acoff [24]. Other researchers that have observed this phenomenon have speculated that they could be unmelted particles within large non-spherical voids [25,26]. Further, Seifi et al. observed this phenomenon in both build directions and concluded that the defect is a lack of fusion defect and its spatial distribution has an influence on the fracture toughness [26]. The dendrites in the present study would suggest that there were regions of the horizontal build specimen that did not solidify at the same rate. This phenomenon was not observed in the vertical sample.

4.4 Conclusions

In this paper, the preferential growth of β phase as a function of build direction was found to have a profound effect on mechanical properties of EBAM Ti-64. The main conclusions include:

- The β-phase was present in a higher concentration in the wrought processed Ti-64 than either of the EBAM specimens.
- The vertical build specimen contained more of the β-phase than the horizontal build. This resulted in the horizontal build to have higher hardness values as well as estimated yield strength and elastic modulus than the vertical EBAM.
- Both builds show evidence of mostly brittle failure with some ductile.

- Evidence of what is believed to be regions that solidified at a different rate were observed in the horizontal build. This resulted in fracture surfaces exposing rounded dendrite surfaces. The observed defects are not believed to be unmelted powders, because their size suggests they could be dendrites that form due to an uneven solidification rate.

References

[1] R. R. Boyer, "An Overview on the Use of Titanium in the Aerospace Industry," *Materials Science and Engineering: A* 213 (1996) 103-114.

[2] A. Majorell, S. Srivatsa and R. R. Picu, "Mechanical Behavior of Ti-6Al-4V at High and Moderate Temperatures," *Materials Science and Engineering: A* 326 (2002) 297 297-305.

[3] J. L. Barreda, F. Santamaría, X. Azpiroz, A. M. Irisarri and J. M. Varona, "Electron beam welded high thickness Ti6Al4V plates using filler metal of similar and different composition to the base plate," *Vacuum* 62 (2001) 143 143-150.

[4] S. Wang and X. Wu, "Investigation on the microstructure and mechanical properties of Ti–6Al–4V alloy joints with electron beam welding," *Materials & Design* 36 (2012) 663-670.

[5] R. Ding, Z. X. Guo and A. Wilson, "Microstructural Evolution of a Ti–6Al–4V Alloy During Thermomechanical Processing," *Materials Science and Engineering: A* 327 (2002) 233-245.

[6] S. Roy and S. Suwas, "Effect of Hypoeutectic Boron Addition on the beta Transus of Ti6Al4V Alloy," *Metallurgical and Materials Transactions A* 42A (2011) 2535-2541.

[7] T. Ahmed and H. Rack, "Phase transformations during cooling in α+ β titanium alloys," *Materials Science and Engineering: A* 243 (1998) 206-211.

[8] Y. Fan, P. Cheng, Y. Yao, Z. Yang and K. Egland, "Effect of phase transformations on laser forming of Ti–6Al–4V alloy," *Journal of applied physics* 98 (2005) 013518.

[9] W. E. Frazier, "Metal Additive Manufacturing: A Review," *Journal of Materials Engineering and Performance* 23 (2014) 1917-1928.

[10] V. Petrovic, J. Vicente Haro Gonzalez, O. Jordá Ferrando, J. Delgado Gordillo, J. Ramón Blasco Puchades and L. Portolés Griñan, "Additive layered manufacturing: sectors of industrial application shown through case studies," *International Journal of Production Research* 49 (2011) 1061-1079.

[11] S. Biamino, A. Penna, U. Ackelid, S. Sabbadini, O. Tassa, P. Fino, M. Pavese, P. Gennaro and C. Badini, "Electron beam melting of Ti–48Al–2Cr–2Nb alloy: Microstructure and mechanical properties investigation," *Intermetallics* 19 (2011) 776-781.

[12] L. E. Murr, S. M. Gaytan, D. A. Ramirez, E. Martinez, J. Hernandez, K. N. Amato, P. W. Shindo, F. R. Medina and R. B. Wicker, "Metal Fabrication by Additive Manufacturing Using Laser and Electron Beam Melting Technologies," *Journal of Materials Science & Technology* 28 (2012) 1-14.

[13] L. E. Murr, E. Martinez, K. N. Amato, S. M. Gaytan, J. Hernandez, D. A. Ramirez, P. W. Shindo, F. Medina and R. B. Wicker, "Fabrication of Metal and Alloy Components by Additive Manufacturing: Examples of 3D Materials Science," *Journal of Materials Research and Technology* 1 (2012) 42-54.

[14] A. Safdar, L. Y. Wei, A. Snis and Z. Lai, "Evaluation of microstructural development in electron beam melted Ti-6Al-4V," *Materials Characterization* 65 (2012) 8-15.

[15] K. P. Rao, K. Angamuthu and P. B. Srinivasan, "Fracture toughness of electron beam welded Ti6Al4V," *Journal of Materials Processing Technology* 199 (2008) 185-192.

[16] P. Zhang, S. Li and Z. Zhang, "General relationship between strength and hardness," *Materials Science and Engineering: A* 529 (2011) 62-73.

[17] P. Sanders, C. Youngdahl and J. Weertman, "The strength of nanocrystalline metals with and without flaws," *Materials Science and Engineering: A* 234 (1997) 77-82.

[18] L. Lu, R. Schwaiger, Z. Shan, M. Dao, K. Lu and S. Suresh, "Nano-sized twins induce high rate sensitivity of flow stress in pure copper," *Acta materialia* 53 (2005) 2169-2179.

[19] S. L. R. da Silva, L. O. Kerber, L. Amaral and C. A. dos Santos, "X-ray diffraction measurements of plasma-nitrided Ti–6Al–4V," *Surface and Coatings Technology* 116-119 (1999) 342-346.

[20] M. Koike, K. Martinez, L. Guo, G. Chahine, R. Kovacevic and T. Okabe, "Evaluation of titanium alloy fabricated using electron beam melting system for dental applications," *Journal of Materials Processing Technology* 211 (2011) 1400-1408.

[21] L. Facchini, E. Magalini, P. Robotti and A. Molinari, "Microstructure and mechanical properties of Ti-6Al-4V produced by electron beam melting of pre-alloyed powders," *Rapid Prototyping Journal* 15 (2009) 171-178.

[22] O. L. Rodriguez, P. G. Allison, W. R. Whittington, D. K. Francis, O. G. Rivera, K. Chou, X. Gong, T. Butler and J. F. Burroughs, "Dynamic tensile behavior of electron beam additive manufactured Ti6Al4V," *Materials Science and Engineering: A* 641 (2015) 323-327.

[23] L. E. Murr, S. A. Quinones, S. M. Gaytan, M. I. Lopez, A. Rodela, E. Y. Martinez, D. H. Hernandez, E. Martinez, F. Medina and R. B. Wicker, "Microstructure and mechanical behavior of Ti-6Al-4V produced by rapid-layer manufacturing, for biomedical applications," *Journal of the mechanical behavior of biomedical materials* 2 (2009) 20-32.

[24] S. W. Howell and V. L. Acoff, "An Investigation of Weld Fracture Surfaces and Mechanical Properties of Two Gamma Titanium Aluminide Alloys," *Practical Failure Analysis* 3 (2003) 63-73.

[25] C. de Formanoir, S. Michotte, O. Rigo, L. Germain and S. Godet, "Electron beam melted Ti–6Al–4V: Microstructure, texture and mechanical behavior of the as-built and heat-treated material," *Materials Science and Engineering: A* 652 (2016) 105-119.

[26] M. Seifi, A. Salem, D. Satko, J. Shaffer and J. J. Lewandowski, "Defect distribution and microstructure heterogeneity effects on fracture resistance and fatigue behavior of EBM Ti–6Al–4V," *International Journal of Fatigue* 94 (2017) 263-287.

CHAPTER 5

CRYSTALLOGRAPHIC TEXTURE ANALYSIS OF TI-6AL-4V COMPONENTS MADE BY ELECTRON BEAM ADDITIVE MANUFACTURING

Abstract

In titanium alloys, solidification conditions in EBAM usually lead to a coarse columnar β-grain structures. Mechanical properties of Ti alloys are closely related to their microstructures. While there are studies being conducted to better understand the mechanical properties that result from the EBAM process, this study aims to better understand the final microstructural texture. This study uses electron backscatter diffraction (EBSD) to gain insight into the crystallographic texture of Ti-64 components processed using EBAM. This study also demonstrates post-processing software to gain insight into simulated grain boundary characteristics of EBAM Ti-64.

5.1 Introduction

EBAM is one of the few AM technologies capable of making full-density metallic parts and has therefore dramatically extended the applications of EBAM [1-5]. EBAM represents a promising opportunity to increase the use of titanium alloys due to its process versatility and flexibility, the non-reactive environmental requirements, and its rapid processing. A detailed description of the overall EBAM process can be found in literature [1,2,4,6-8].

Ti-6Al-4V (Ti-64) is by far the most widely used titanium alloy due to its versatile combination of strength and other mechanical properties that it retains even at high temperatures. Because of this, Ti-64 has seen high usage in the aeronautics and aerospace industries, but due to its biological and chemical inertness it has also seen use both the medical and dental industries [9-11]. Ti-64 is a typical dual-phase alloy comprised of α HCP + β BCC where the α phase normally precipitates in β matrix with the classic Burgers relationship $(0001)_\alpha$ //$(110)_\beta$, $[10\bar{2}0]_\alpha$ //$[111]_\beta$ [12,13]. At room temperature the alloy is comprised mostly α, but at the β transus temperature around 980-996 °C [14] the β-phase becomes completely stable up to the melting point [15]. A cooling rate faster than (137 °C/s [16,17]) from the homogeneous β produces martensitic α-phases [18]. However, if there is a slower cooling rate below the β transus temperature, grain boundary α-phase may grow at the β-grain boundaries or a plate-like α structure may form within the prior β grains at lower temperatures [19]. The plate-like α structure is known as Widmanstätten.

The mechanical properties of titanium alloys are dependent on the microstructure, which is determined by the thermo-mechanical processing and thermal treatment. Previous work has shown that the EBAM built parts are overall superior mechanically than wrought form [7,12]. In a study of mechanical anisotropy of EBAM Ti-64 conducted by Ladani et al. [20] it has been

suggested that the horizontal built specimens have a greater tensile strength and microhardness compared to other build directions. The main focus of this study is to investigate microstructural features, specifically crystallographic texture, of EBAM processed Ti-64 via electron back scattered diffraction (EBSD) and Matlab Texture (MTEX) and draw a direct comparison to wrought Ti-64.

In a polycrystalline material, texture is defined as the preferred orientation of constituent grains; and further, each grain is arranged in an order that is based on the structure of the metal. To represent the relationship between the grain orientation and its axis, the normal direction (ND), rolling direction (RD) and transversal direction (TD) are used. For the purposes of this work, build direction (BD) and ND are synonymous, and scanning direction (SD) will be used instead of RD as shown in Figure 5.1.

5.2 Experimental Materials and Procedures

For this work, all EBAM Ti-64 parts were fabricated from Ti-64 powders at NASA Marshall Space Flight Center in Huntsville, Alabama using the Arcam S12 EBM system at an accelerating voltage of 60Kv, a beam current of 5mA, and a scanning speed of 200 mm/s. Samples with specific build directions (e.g. vertical and horizontal) were used, as illustrated in Figure 5.1. The specimens were prepared for scanning electron microscopy (1μm spot size, 18KV) analysis using standard metallographic procedures, including grinding up to 800 grit SiC papers, followed by polishing using diamond suspension of 3, 1, and 0.05μm. As titanium and its alloys are notoriously difficult to polish well enough for EBSD, the samples were vibratory polished in 0.05 μm diamond suspension for 6 hours. For this study, all post-processing and analysis was performed using MTEX and the Oxford Instrument grain analysis. MTEX is a free

Matlab toolbox for analyzing and modeling crystallographic texture using data from EBSD or pole figures (PFs).

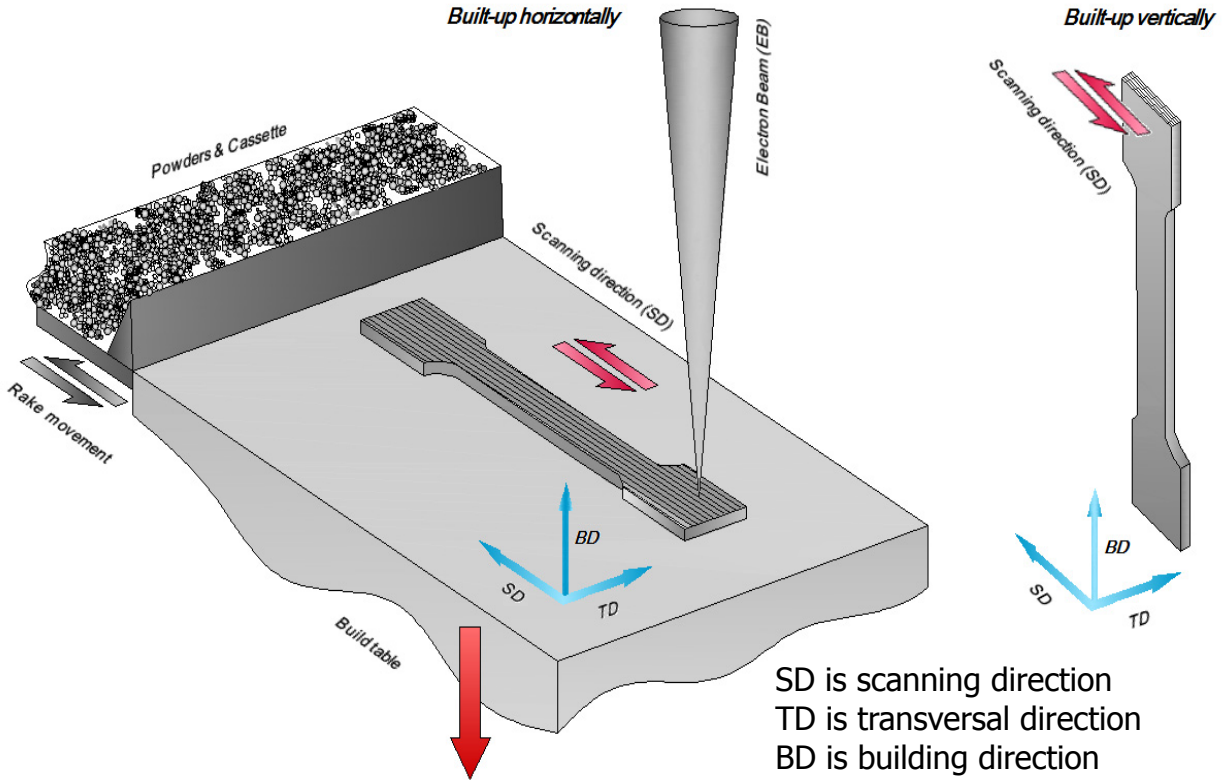

Figure 5.1 Schematic of S12 Arcam EBAM machine at NASA MSFC.

5.3 Results and Discussion

Figures 5.2 – 5.6 shows the experimental band contrast images with the β-phase imposed in red and inverse pole figure (IPF) maps for wrought, horizontal EBAM, and vertical EBAM respectively. In Figure 5.2, the image is dominated by blue indicating a preference to the <111>. Figures 5.3 and 5.4 are of the horizontal EBAM builds. In both horizontal builds, there is a strong columnar grain structure. In the SD-BD horizontal build shown in Figure 5.3, the image is dominated by the green color indicating a preference to the $<2\bar{1}\bar{1}0>$. In Figure 5.4 the image has a strong presence of green and pink. There is also a strong yellow presence in the lower right quadrant. Figures 5.5 and 5.6 are of the vertical EBAM builds. Both vertical builds exhibit a somewhat randomized equiaxed grain structure. The BD-TD section shown in Figure 5.5 is dominated by the orange color, which is near <0001> for hexagonal and <001> for cubic. The SD-TD shown in Figure 5.6 is not dominated by any single color, however the purple and green appear to be present in nearly equal amounts which suggests no strong orientation preference.

In an early iteration of EBSD data, there were several peaks that the EBSD software could not index. Thus MTEX was used to remove the unindexed points and take the mean of the nearby indexed orientations to extrapolate the data in the models. The band contrast images from the experimental data as well as the MTEX generated IPF maps are shown in Figure 5.7. The MTEX generated images are reflections of the band contrast images, and because of angle threshold limitations in the software, not all grain boundaries could be resolved. MTEX was also able to generate pole figures of our post processed data. The $\{10\bar{1}0\}$, $\{11\bar{2}0\}$, and $\{11\bar{2}1\}$ pole figures are displayed in Figure 5.8. The pole figures for the wrought and horizontal built EBAM Ti-64 appear to be similar except for some shifting in the x direction.

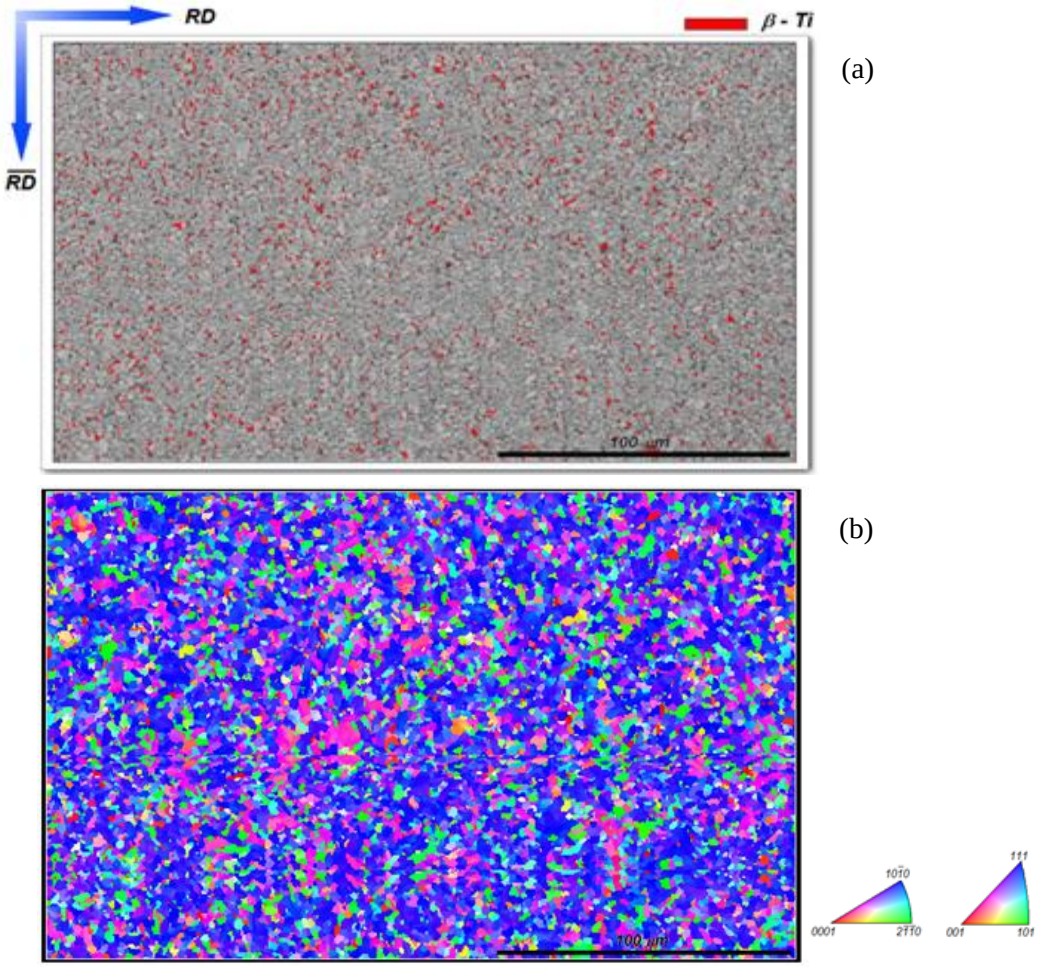

Figure 5.2 Band contrast (a) and IPF map (b) of wrought Ti-64.

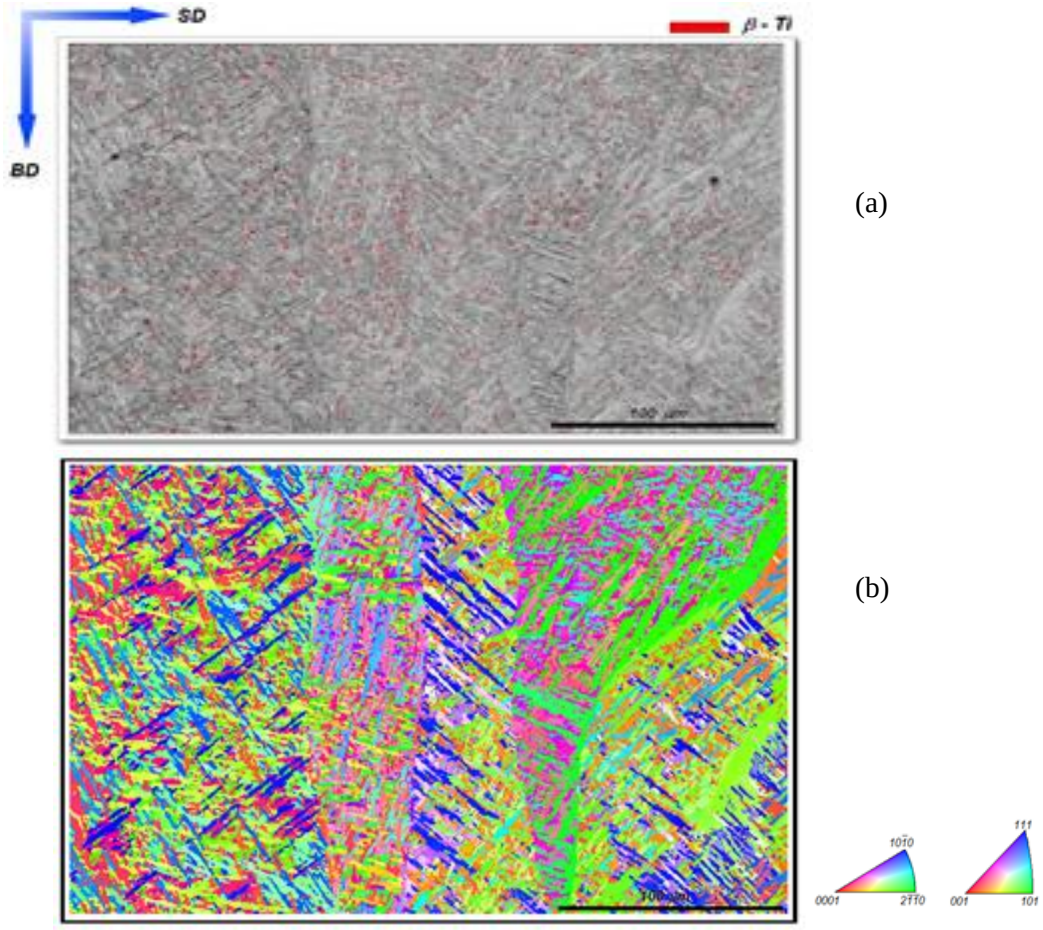

Figure 5.3 Band contrast image (a) and IPF map (b) of SD-BD section of horizontal EBAM Ti-64.

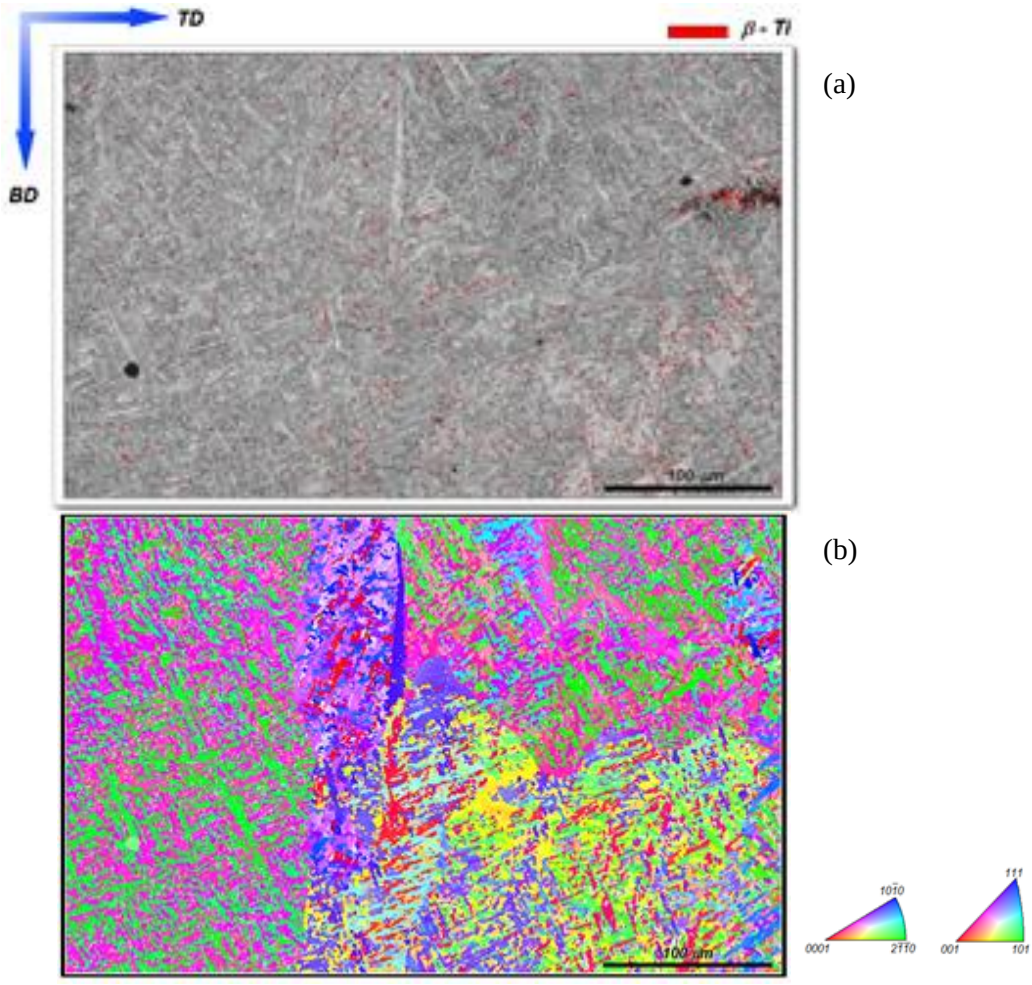

Figure 5.4 Band contrast image (a) and IPF map (b) of TD-BD section of horizontal EBAM Ti-64.

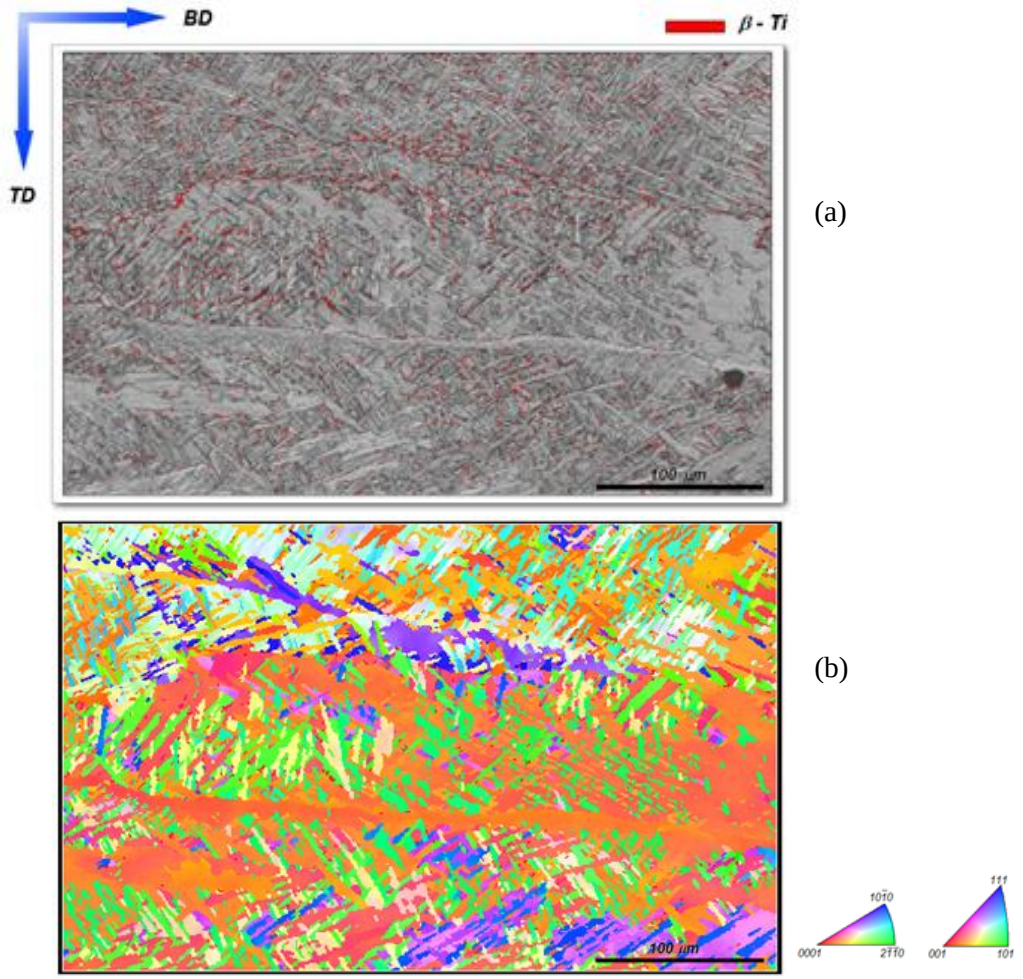

Figure 5.5 Band contrast image (a) and IPF map (b) of BD-TD section of vertical EBAM Ti-64.

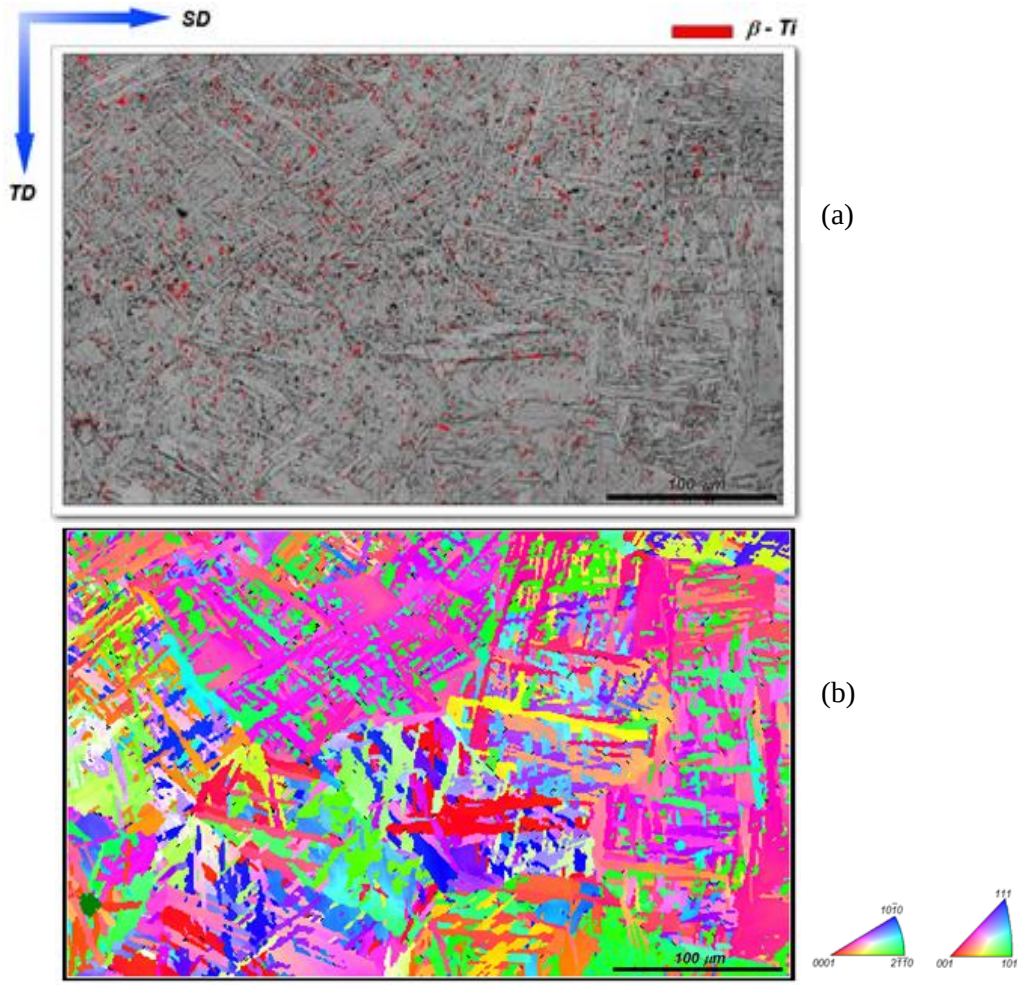

Figure 5.6 Band contrast image (a) and IPF map (b) of SD-TD section of vertical EBAM Ti-64.

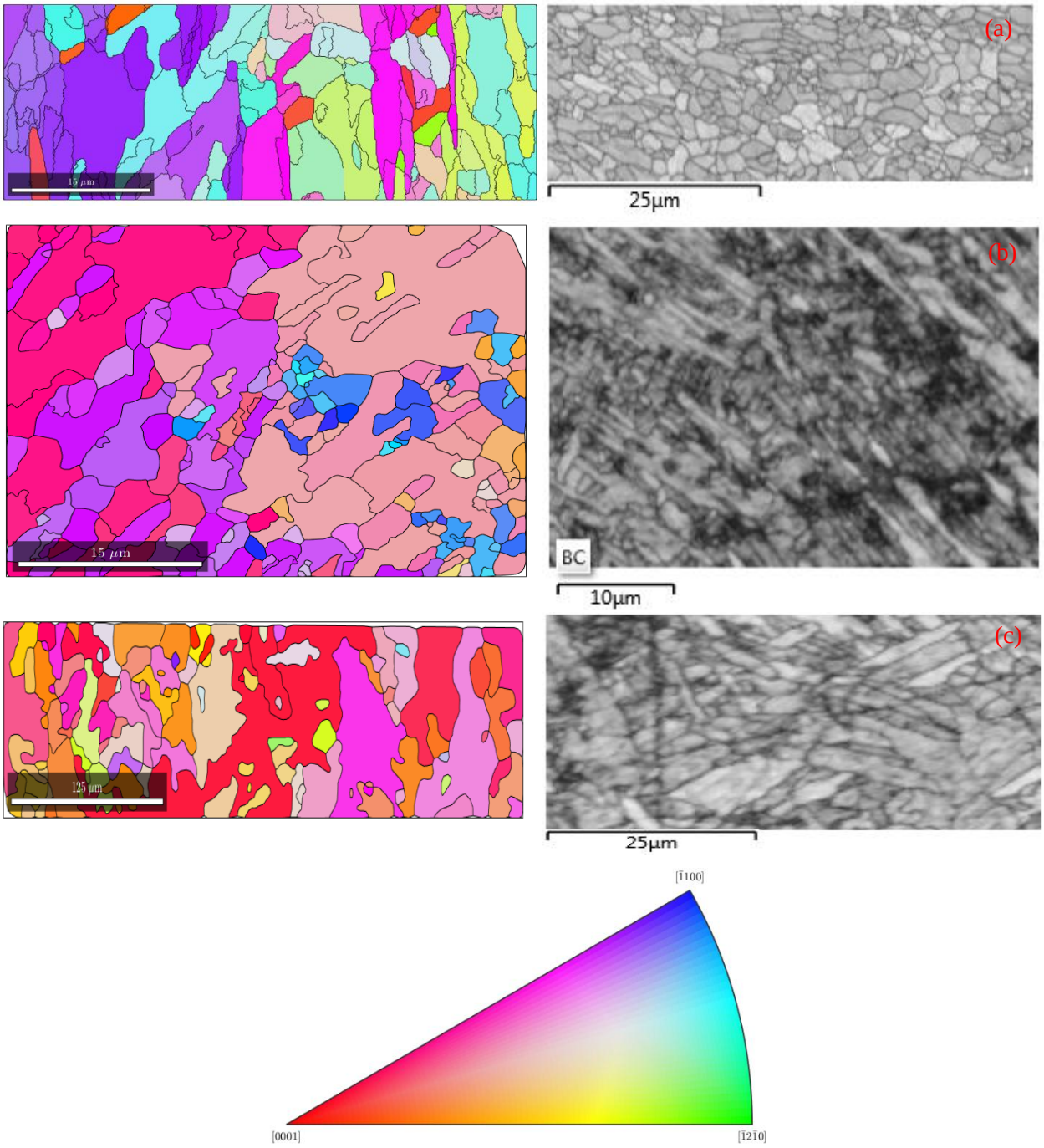

Figure 5.7 Band contrast images and MTEX generated IPF maps of (a) wrought, (b) horizontal EBAM, and (c) vertical EBAM Ti-64.

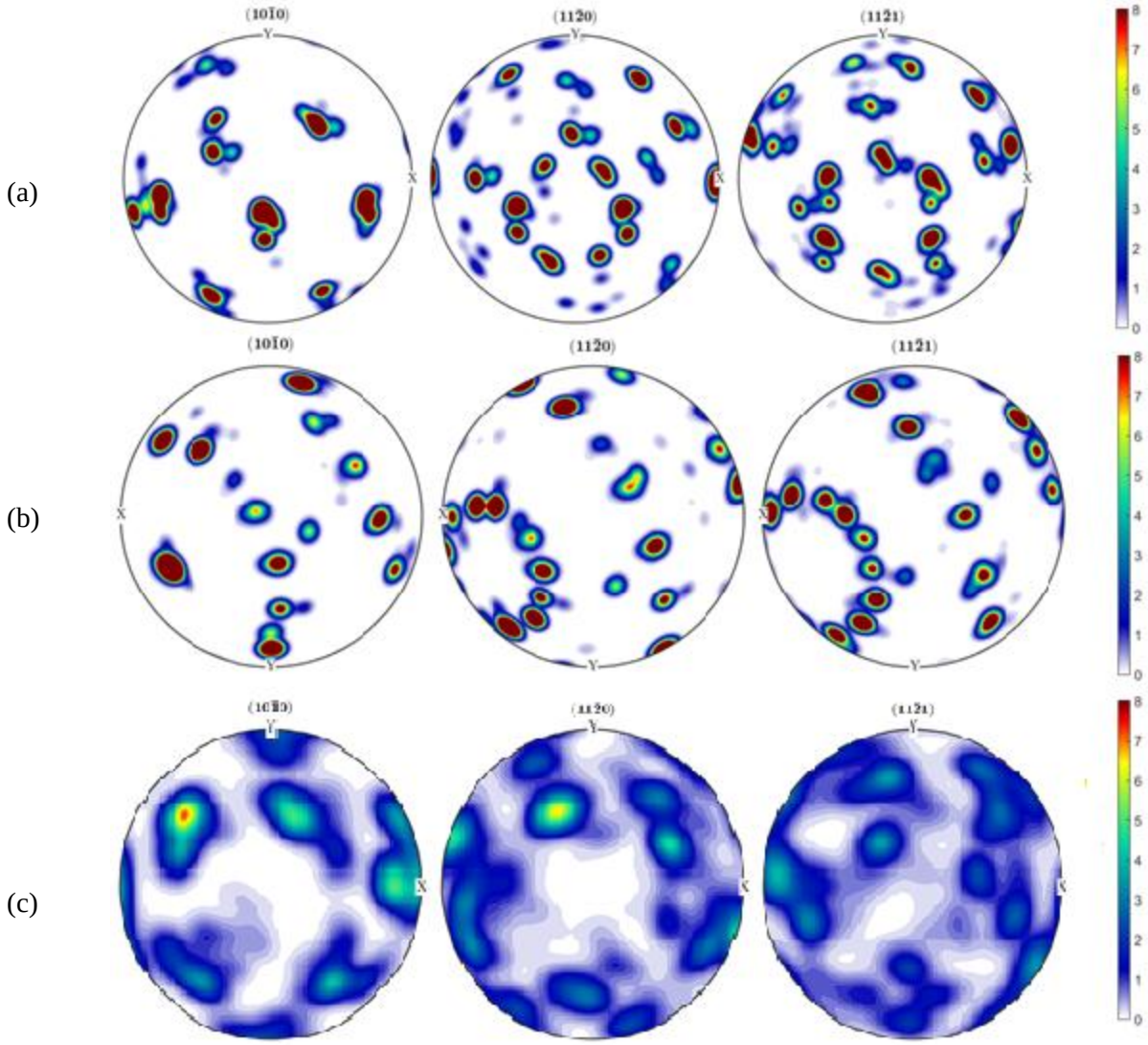

Figure 5.8 Respective MTEX generated pole figures of (a) wrought (b) EBAM horizontal, and (c) EBAM vertical.

Grain boundaries (GBs) are defects in the crystal structure that can affect many physical properties of materials. One well known example of grain boundaries directly impacting a physical property is the Hall-Petch relationship [12,21] which describes that a reduction in grain size will coincide with an increase in yield strength. To characterize GBs, two methods are commonly utilized: misorientation angles [22] and coincident site lattice (CSL) theory [23]. Misorientation in GBs is described as the difference in crystallographic orientation between adjacent crystals in a polycrystalline material. Figure 5.9 displays the networks of the samples in which each of the GBs are colored according to its GB misorientation angle. Figure 5.10 shows the frequency of respective misorientation angles from Figure 5.9. It is shown that the wrought sample is dominated by low angle grain boundaries (LAGB), which are typically defined as any angle below 15°. This was not the case for either of the EBAM samples, although the horizontal sample has LAGBs occurring significantly more than the vertical EBAM. Each of the samples have a sharp increase in frequency at 60°.

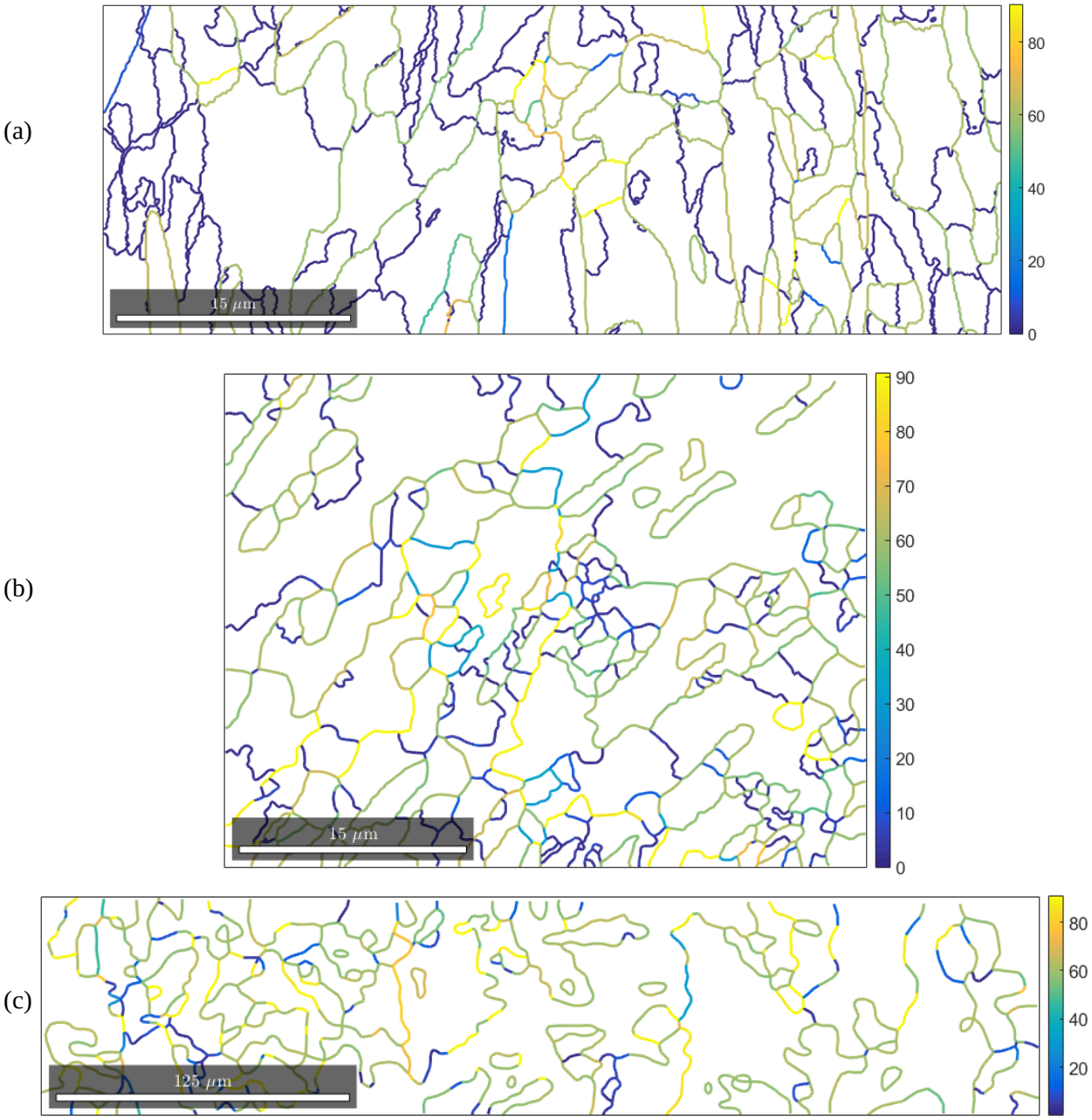

Figure 5.9 Misorientation networks of (a) wrought, (b) horizontal built, and (c) vertical built EBAM.

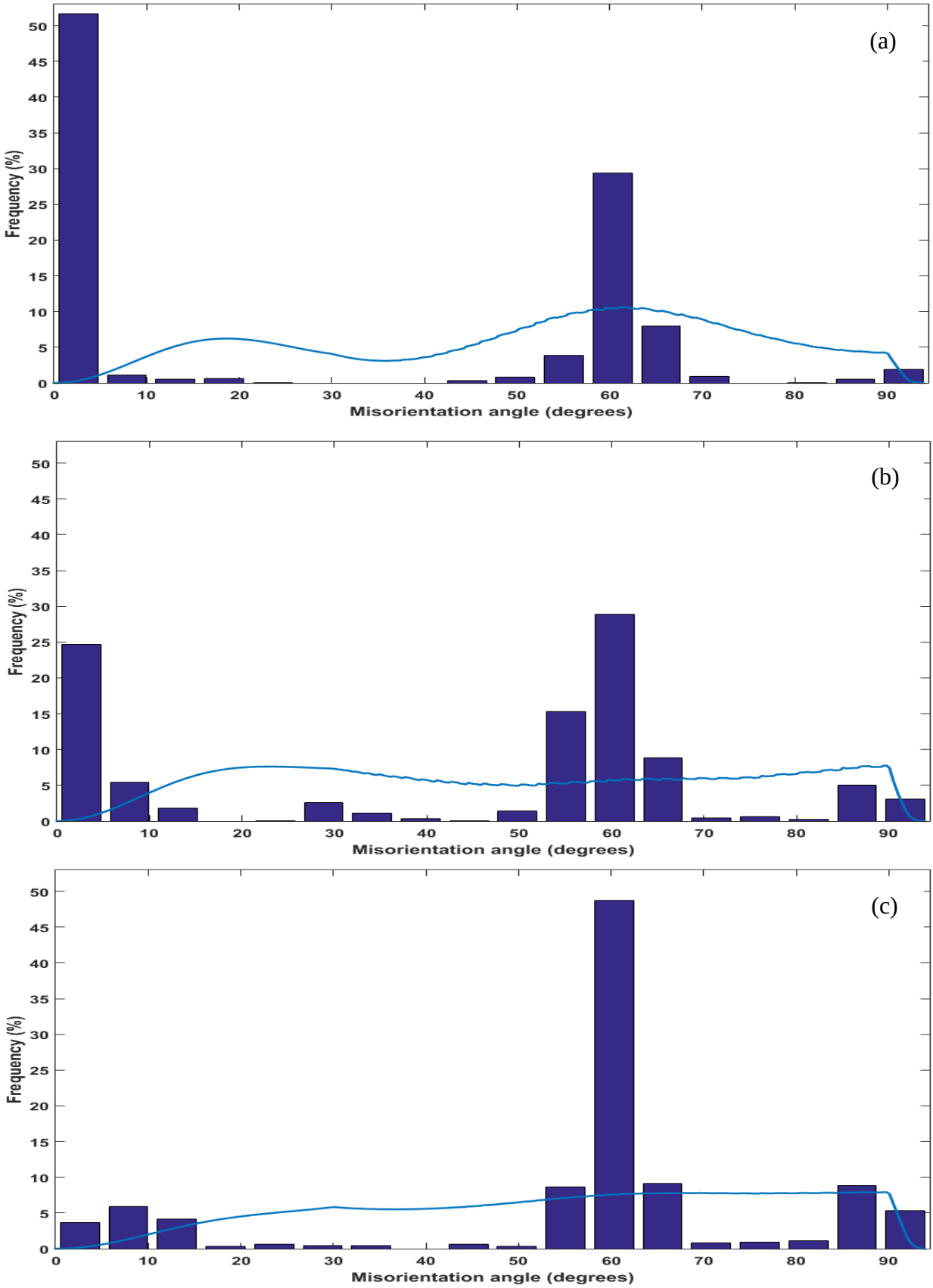

Figure 5.10 Misorientation distribution (a) wrought, (b) horizontal built EBAM, and (c) vertical built EBAM.

CSL theory is a geometric concept used to simplify the large parameter space associated with GB crystallography into a scalar quantity [24]. CSL is a model that is used to describe the combinations of misorientations that exist such that an interface has certain correlations within the formed crystal. In simplest terms, CSL attempts to map special GBs. Figure 5.11 displays the networks CSL boundaries of the GB networks. Analyzing the GB network special boundaries (defined as boundaries CSL$\leq$ 21) are of particular interest. Table 5.1 shows a comparison of special vs general (CSL$>$ 21). Although, there are no twin boundaries in any of the samples, the horizontal EBAM sample exhibits a substantial amount of special boundary length when compared to the wrought and vertical EBAM, this is the inverse of the trend shown earlier with the concentration of the β-phase. This relationship between the GB length and the amount of β-phase present in the material may be useful for GB engineering in future studies to see if a relationship exists between general/special GBs and β growth and mechanical properties.

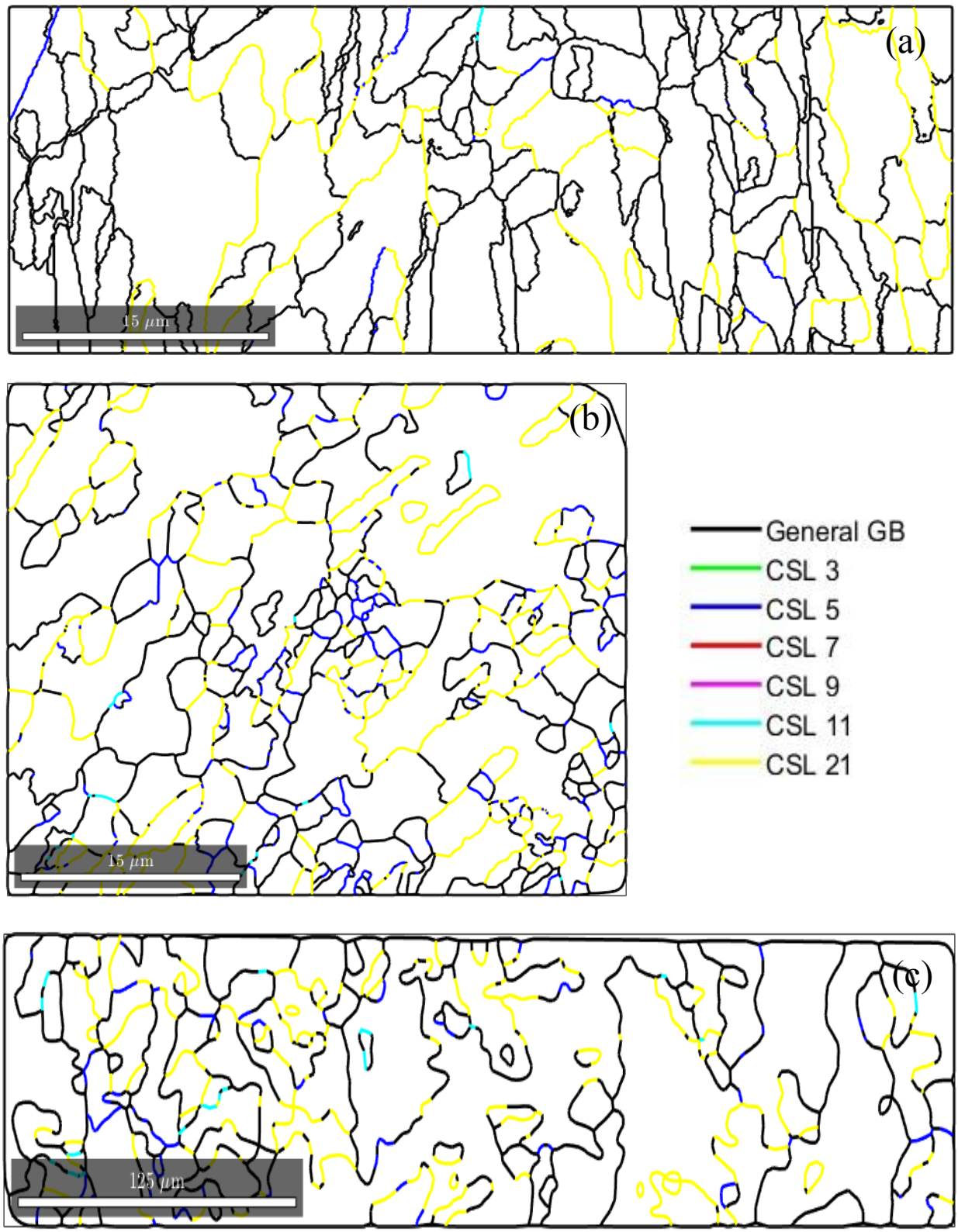

Figure 5.11 CSL boundaries of the GB networks of (a) wrought, (b) horizontal EBAM, and (c) vertical EBAM

Table 5.1 Special GB length vs. General GB length.

	Fraction of General GBs	Fraction of CSL
Wrought	0.7266	0.2734
Horizontal EBAM	0.4980	0.5020
Vertical EBAM	0.6635	0.3365

5.4 Conclusions

In this study, the microstructure of wrought Ti-64 was compared to that of different build directions of EBAM Ti-64. The main conclusions include:

- The microstructures of the EBAM Ti-64 samples we studied showed no preferential grain orientation.
- The wrought Ti-64 is primarily composed of LAGBs, this is not the case for either build direction of the EBAM samples, especially the vertical build.
- There were no twin boundaries in any of the samples, however the horizontal EBAM exhibited a substantial amount of special boundary length in comparison to the vertical EBAM and wrought Ti-64.

References

[1] W. E. Frazier, "Metal Additive Manufacturing: A Review," *Journal of Materials Engineering and Performance* 23 (2014) 1917-1928.

[2] V. Petrovic, J. Vicente Haro Gonzalez, O. Jordá Ferrando, J. Delgado Gordillo, J. Ramón Blasco Puchades and L. Portolés Griñan, "Additive layered manufacturing: sectors of industrial application shown through case studies," *International Journal of Production Research* 49 (2011) 1061-1079.

[3] S. Biamino, A. Penna, U. Ackelid, S. Sabbadini, O. Tassa, P. Fino, M. Pavese, P. Gennaro and C. Badini, "Electron beam melting of Ti–48Al–2Cr–2Nb alloy: Microstructure and mechanical properties investigation," *Intermetallics* 19 (2011) 776-781.

[4] L. E. Murr, S. M. Gaytan, D. A. Ramirez, E. Martinez, J. Hernandez, K. N. Amato, P. W. Shindo, F. R. Medina and R. B. Wicker, "Metal Fabrication by Additive Manufacturing Using Laser and Electron Beam Melting Technologies," *Journal of Materials Science & Technology* 28 (2012) 1-14.

[5] L. E. Murr, E. Martinez, K. N. Amato, S. M. Gaytan, J. Hernandez, D. A. Ramirez, P. W. Shindo, F. Medina and R. B. Wicker, "Fabrication of Metal and Alloy Components by Additive Manufacturing: Examples of 3D Materials Science," *Journal of Materials Research and Technology* 1 (2012) 42-54.

[6] J. Hiemenz, "Electron beam melting," *Adv Mater Processes* 165 (2007) 45-46.

[7] X. Gong, T. Anderson and K. Chou, "Review on powder-based electron beam additive manufacturing technology," *Manufacturing Review* 1 (2014) 2.

[8] L. E. Murr, E. V. Esquivel, S. A. Quinones, S. M. Gaytan, M. I. Lopez, E. Y. Martinez, F. Medina, D. H. Hernandez, E. Martinez, J. L. Martinez, S. W. Stafford, D. K. Brown, T. Hoppe, W. Meyers, U. Lindhe and R. B. Wicker, "Microstructures and mechanical properties of electron beam-rapid manufactured Ti–6Al–4V biomedical prototypes compared to wrought Ti–6Al–4V," *Materials Characterization* 60 (2009) 96-105.

[9] R. R. Boyer, "An Overview on the Use of Titanium in the Aerospace Industry," *Materials Science and Engineering: A* 213 (1996) 103-114.

[10] A. Majorell, S. Srivatsa and R. R. Picu, "Mechanical Behavior of Ti-6Al-4V at High and Moderate Temperatures," *Materials Science and Engineering: A* 326 (2002) 297 297-305.

[11] J. L. Barreda, F. Santamaría, X. Azpiroz, A. M. Irisarri and J. M. Varona, "Electron beam welded high thickness Ti6Al4V plates using filler metal of similar and different composition to the base plate," *Vacuum* 62 (2001) 143 143-150.

[12] X. Tan, Y. Kok, Y. J. Tan, M. Descoins, D. Mangelinck, S. B. Tor, K. F. Leong and C. K. Chua, "Graded microstructure and mechanical properties of additive manufactured Ti–6Al–4V via electron beam melting," *Acta Materialia* 97 (2015) 1-16.

[13] L.-q. Yang and Y.-q. Yang, "Deformed microstructure and texture of Ti6Al4V alloy," *Transactions of Nonferrous Metals Society of China* 24 (2014) 3103-3110.

[14] R. Ding, Z. X. Guo and A. Wilson, "Microstructural Evolution of a Ti–6Al–4V Alloy During Thermomechanical Processing," *Materials Science and Engineering: A* 327 (2002) 233-245.

[15] S. Roy and S. Suwas, "Effect of Hypoeutectic Boron Addition on the beta Transus of Ti6Al4V Alloy," *Metallurgical and Materials Transactions A* 42A (2011) 2535-2541.

[16] T. Ahmed and H. Rack, "Phase transformations during cooling in α+ β titanium alloys," *Materials Science and Engineering: A* 243 (1998) 206-211.

[17] Y. Fan, P. Cheng, Y. Yao, Z. Yang and K. Egland, "Effect of phase transformations on laser forming of Ti–6Al–4V alloy," *Journal of applied physics* 98 (2005) 013518.

[18] T. Ahmed and H. J. Rack, "Phase transformations during cooling in a b titanium alloys." (1998). 243

[19] C. C. Murgau, R. Pederson and L. E. Lindgren, "A model for Ti–6Al–4V microstructure evolution for arbitrary temperature changes," *Modelling and Simulation in Materials Science and Engineering* 20 (2012) 055006.

[20] L. Ladani, J. Razmi and S. Farhan Choudhury, "Mechanical Anisotropy and Strain Rate Dependency Behavior of Ti6Al4V Produced Using E-Beam Additive Fabrication," *J. Eng. Mater. Technol.* 136 (2014).

[21] R. W. Armstrong, "Engineering science aspects of the Hall–Petch relation," *Acta Mechanica* 225 (2014) 1013-1028.

[22] V. Randle, H. Davies and I. Cross, "Grain boundary misorientation distributions," *Current Opinion in Solid State and Materials Science* 5 (2001) 3-8.

[23] D. H. Warrington and P. Bufalini, "The Coincidence Site Lattice and Grain Boundaries," *Scripta Metallurgica* 5 (1971) 771-776.

[24] A. Santoro and A. D. Mighell, "Coincidence Site Lattices," *Acta Crystallographica A* 29 (1973) 169-175.

CHAPTER 6

CONCLUSIONS AND FUTURE WORK

6.1 Major Conclusions

The microstructure and mechanical properties of Ti-64 were studied in an effort to draw a direct comparison between wrought and EBAM with different build directions. The main conclusions are as follows:

(1) The microstructures of the wrought sample expectedly showed α grains and an intergranular β phase. The EBAM microstructures showed the martensitic needle structure from within the prior β grains.

(2) The EBAM process increases the microhardness of Ti-64 compared to the wrought sample. This can be attributed to the formation of the α′ phase present in the EBAM samples which is harder compared to both the α and β phases present in the base metal.

(3) The β-phase is present in a higher concentration in wrought processed Ti-64 than in either of the EBAM specimens. The vertical build contained more of the β-phase than the horizontal build and that caused the horizontal build to have a higher microhardness than both the vertical EBAM and wrought Ti-64.

(4) Both builds show evidence of mostly brittle failures with some ductile.

(5) Defects formed along the fracture surfaces of the horizontal build. This was not present in the vertical build. The observed defects could be unmelted powders, but their size suggest they could be dendrites that form due to an uneven solidification rate

(6) The microstructures of the EBAM Ti-64 samples we studied showed no preferential grain orientation.

(7) The wrought Ti-64 is primarily composed of LAGBs. This is not the case for either build direction of the EBAM samples, especially the vertical build.

(8) There were no twin boundaries in any of the samples, however the horizontal EBAM exhibited a substantial amount of special boundary length in comparison to the vertical EBAM and wrought Ti-64.

(9) The horizontal EBAM has higher special GB length.

6.2 Recommendation for Future Work

(1) GBs are susceptible to corrosion [1-3]. It has been shown that the EBAM process alters the microstructure of Ti-64 and these microstructural changes improve many of the mechanical properties. It would be very interesting to determine if the EBAM process has any effect on the corrosion resistance of Ti-64.

(2) The GB network special boundaries were studied and it was found that there were no twin boundaries in any of the specimens. However the horizontal sample showed a higher fraction of special GB lengths when compared to the wrought or vertical samples. Properties of polycrystalline materials are often influenced by the character and connectivity of GB, thus a thorough GB engineering study is necessary.

(3) A detailed texture study is recommended.

References

[1] G. Palumbo and K. T. Aust, "Structure-dependence of Intergranular Corrosion in High Purity Nickel," *Acta Metallurgica et Materialia* 38 (1990) 2343-2352.

[2] P. Lin, G. Palumbo, U. Erb and K. T. Aust, "Influence of grain boundary character distribution on sensitization and intergranular corrosion of alloy 600," *Scripta Metallurgica et Materialia* 33 (1995) 1387-1392.

[3] E. M. Lehockey, D. Limoges, G. Palumbo, J. Sklarchuk, K. Tomantschger and A. Vincze, "On Improving the Corrosion and Growth Resistance of Positve Pb-acid Battery Grids by Grain Boundary Engineering," *Journal of Power Sources* 78 (1999) 79-83.